Transcriptomic analysis of meiotic genes during the mitosis-to-meiosis transition in *Drosophila* females

Ana Maria Vallés[1*], Thomas Rubin[1*], Nicolas Macaisne[1a], Laurine Dal Toe[1b], Anahi Molla-Herman[1], Christophe Antoniewski[2] and Jean-René Huynh[1&]

1 Collège de France, PSL Research University, CNRS, Inserm, Center for Interdisciplinary Research in Biology, Paris, France

2 ARTbio Bioinformatics Analysis Facility, IBPS, CNRS, Sorbonne Université, Institut Français de Bioinformatique, Paris, France.

* equal contribution

&Corresponding author: jean-rene.huynh@college-de-france.fr

a present address: Université Paris Cité, CNRS, Institut Jacques Monod, F-75013 Paris, France.
b present address: CBS, Univ Montpellier, CNRS, INSERM, Montpellier, France

Keywords: germline, oocyte, Spo11, recombination, cell cycle, development.

Abstract

Germline cells produce gametes, which are specialized cells essential for sexual reproduction. Germline cells first amplify through several rounds of mitosis before switching to the meiotic program, which requires specific sets of proteins for DNA recombination, chromosome pairing and segregation. Surprisingly, we previously found that some proteins of the synaptonemal complex, a prophase I meiotic structure, are already expressed and required in the mitotic region of *Drosophila* females. Here, to assess if additional meiotic genes were expressed earlier than expected, we isolated mitotic and meiotic cell populations to compare their RNA content. Our transcriptomic analysis reveals that all known meiosis I genes are already expressed in the mitotic region, however, only some of them are translated. As a case study, we focused on *mei-W68*, the *Drosophila* homologue of *Spo11*, to assess its expression at both the mRNA and protein levels, and used different mutant alleles to assay for a pre-meiotic function. We could not detect any functional role for Mei-W68 during homologous chromosome pairing in dividing germ cells. Our study paves the way for further functional analysis of meiotic genes expressed in the mitotic region.

Article Summary

Germline cells, crucial for sexual reproduction, were thought to switch to meiosis only after several rounds of mitosis. Surprisingly, a few meiotic proteins were found active in the mitotic phase of female flies. Here, we discovered that all known meiosis genes were expressed during mitosis, but only some produced proteins. This study suggests that genes related to reproduction are active earlier than expected, prompting further exploration into their functions during early cell division.

Introduction

In organisms reproducing sexually, germline cells produce oocytes and sperms as gametes. Germline cell differentiation starts by an amplification phase through mitosis to increase their numbers and create a pool of precursor cells (CINALLI *et al.* 2008). They then switch to meiosis, which comprises two rounds of nuclear divisions to produce haploid gametes. Meiosis is specific to germline cells and requires the expression of unique molecular machineries to pair, recombine and segregate homologous chromosomes. How germline cells switch from a mitotic to a meiotic program is not fully understood.

Meiosis starts by an extended prophase I during which homologous chromosomes have to find each other in the nuclear space to pair (BHALLA AND DERNBURG 2008; ZICKLER AND KLECKNER 2015). Once homologous chromosomes are paired, their association is stabilized by the synaptonemal complex (SC), the proteinaceous structure that holds homologous axes together (synapsis) and promotes genetic recombination (CAHOON AND HAWLEY 2016). Recombination starts by the formation of developmentally programmed double-strand breaks (DSBs), which can be later repaired as crossovers. Meiotic DSBs are induced by the topoisomerase-like Spo11, which is conserved in all species (KEENEY *et al.* 1997; DE MASSY 2013). These chromosome exchanges create physical links called chiasmata, which keep homologues paired until they orient towards opposite poles of the spindle. This period is subdivided in five classical stages (leptotene, zygotene, pachytene, diplotene, and diakinesis) based on chromosome morphologies. The initiation of the pairing process has been defined at the early zygotene stage in *Saccharomyces cerevisiae* (TSUBOUCHI T 2005) and at the leptotene stage in *C. elegans* (CRITTENDEN SL 2006; ROHOZKOVA *et al.* 2019) zebrafish (BLOKHINA *et al.* 2019) and mice (ISHIGURO *et al.* 2014; SCHERTHAN *et al.* 2014), by FISH analysis and chromosome axis protein imaging. Moreover, chromosome movements, forces and molecular players that promote pairing have been well characterized by live imaging microscopy in these species (RUBIN *et al.* 2020; KIM *et al.* 2022).

However, we and others have found that homologous chromosomes start to pair through centromeres and euchromatic loci during the mitotic phases preceding leptotene in both *Drosophila* males and females (CAHOON AND HAWLEY 2013; CHRISTOPHOROU N 2013; JOYCE EF 2013; CHRISTOPHOROU *et al.* 2015; RUBIN *et al.* 2022). Moreover, we showed that this pre-meiotic pairing requires components of the synaptonemal complex, a structure specific to prophase I of meiosis (CHRISTOPHOROU N 2013; RUBIN *et al.* 2022). Indeed, the C(3)G and Corona proteins, which form the central region of the SC, are transcribed and translated in the mitotic region and localize on one side of centromeres. It is similar to the initiation of meiosis

in budding yeast, where centromeres become "coupled" before meiotic prophase (TSUBOUCHI T 2005). This early association also depends on Zip1, a central component of the SC functionally similar to C(3)G in flies and SYCP1 in mice. Furthermore, recent analyses in mice have shown that meiotic genes involved in prophase I are expressed and translated long before the initiation of the meiotic process (WANG *et al.* 2001; EVANS *et al.* 2014; ZHENG *et al.* 2022). For example, the meiotic cohesin REC8, as in *C. elegans* (PASIERBEK *et al.* 2001) and synaptonemal complex proteins are expressed and actively translated in spermatogonia, which go through several mitotic divisions before meiotic entry. In addition, Spo11 protein is also found at very low levels in spermatogonia (FANG *et al.* 2021).

Here, to assess if additional meiotic genes were expressed in the mitotic region of *Drosophila* females, we analyzed the whole genome transcriptome of mitotic and meiotic germline cells.

Results

1. Meiotic genes are expressed in the mitotic region

In *Drosophila* females, the processes of mitosis and meiosis occur sequentially throughout the adult life in a structure called the germarium located at the tip of each ovary (SPRADLING 1993). At the anterior-most part is the mitotic zone, also known as region 1. In this zone, germline stem cells (GSCs) proliferate and self-renew by receiving signals from adjacent somatic tissue that induce the expression of stem cell promoting factors like *nanos*, which mediate the translational repression of differentiation genes (SLAIDINA AND LEHMANN 2014). GSCs divide mostly asymmetrically and generate a posterior daughter cell, which differentiates into a precursor cell called cystoblast (CB). The CB undergoes four rounds of mitosis, resulting in the formation of a germline cyst consisting of 16 cells (Figure 1A) (HUYNH AND ST JOHNSTON 2004). During these mitotic divisions, cells remain connected through ring canals and a specialized organelle called the fusome. The branching pattern of the fusome is a useful marker for distinguishing the different stages within the mitotic zone, i.e. GSCs, CBs, and cysts of 2, 4, 8, and 16 cells (DE CUEVAS AND SPRADLING 1998). The period of rapid synchronized divisions marks the transition phase and the commitment to differentiation. The Bag of marble (Bam) protein induces the differentiation of CBs and its expression is spatially restricted: suppressed by self-renewal factors in GSCs and activated in CBs and 2, 4, 8-cell cysts (Fig. 1B and C) (CHEN AND MCKEARIN 2003). After the last mitosis, cysts enter the meiotic zone, also

known as region 2a, where all 16 cells that look identical enter meiosis (CARPENTER 1975). The presence of the synaptonemal complex (SC) in this early meiotic zone marks the initiation of prophase I, with only two pro-oocytes progressing to form a complete SC (HUGHES *et al.* 2018). At this stage, meiotic double-strand breaks (DSBs) are induced. As the cyst reaches region 2b, only one cell within the cyst will become an oocyte, while the remaining 15 cells develop into nurse cells and undergo DNA endoreplication. In this region, the cyst undergoes a significant morphological change, adopting a disc-like shape that is one cell thick and spans the entire width of the germarium. Concomitantly, somatic follicle cells begin to migrate and enclose the cyst. As the cyst advances to region 3, also known as stage 1, it assumes a rounded shape forming a sphere. At late pachytene, the oocyte stage is marked with SC and consistently positioned at the posterior pole. Subsequently, the cyst exits the germarium and enters the vitellarium (HUYNH AND ST JOHNSTON 2004).

Although meiosis is described as beginning in early region 2a of the germarium, several proteins needed for homologous chromosomes pairing are already present in mitotically dividing cells of region 1. The synaptonemal complex protein C(3)G is one example, which localizes near the centromeres of chromosomes II and III and whose expression is required for initiating centromeric pairing ((CHRISTOPHOROU N 2013); Figure 1 B,C). To gain a more exhaustive view of the spatiotemporal expression of meiotic genes, we separated the mitotic and meiotic cell populations by FACS and then processed the RNA for high-throughput sequencing. The separation method relied on the restrictive expression pattern and properties of Bam and Wcd transgenic proteins (VALLES AND HUYNH 2020): Bam::GFP is detectable only in 2-8 cell cysts of region 1 and was used to label the mitotic region (MCKEARIN AND OHLSTEIN 1995). Wcd::RFP has a fast turnover and, when driven by *nanos*-Gal4, it labels a few GSCs, and mostly region 2a/b cells; we therefore used it to identify cells in the first stages of meiosis I. The transgenic line (Bam::GFP; nos>Wcd::RFP) labeled germaria and allowed efficient separation of both mitotic and meiotic germ cell population (see Material and Methods section Figure S1-S3; Table S5). We confirmed the efficiency of cell-sorting by qRT-PCR for specific transcripts. We found that GFP cells were strongly enriched in GFP and *bam* RNA transcripts, while RFP cells were enriched in RFP and *wcd* RNAs (Figure 1D, E). Endogenous Piwi protein was shown to be strongly downregulated in 2- to 8-cell cysts forming a “piwilesspocket (pilp)” (DUFOURT *et al.* 2014). Similarly, we found that *piwi* mRNA levels were lower in the mitotic region compared to the meiotic region (Figure 1D). *matrimony* (*mtrm*) was reported to be very lowly expressed in the mitotic region and higher in the meiotic region by different methods

such as single-cell RNAseq and synchronized germline cells (SLAIDINA *et al.* 2021; SAMUELS *et al.* 2024). We confirmed these results by RT-qPCR and RNAseq (Figure 1D and 1E; Table S1-4). As an additional control, we used *blanks*, as this gene was previously shown to display the opposite trend with higher expression in mitotic cells than in meiotic cells (SLAIDINA *et al.* 2021; SAMUELS *et al.* 2024). Similarly, our results indicate that *blanks* expression levels are higher in the GFP+ cell population than in the RFP+ population (Figure 1E). To evaluate the contamination by other cell types, we searched for somatic cell markers such as *Robo3*, *vnd* (neural cell), *twist* and *bap* (mesoderm) and *dpp*, *egfr*, *STAT92*, which are expressed in somatic cells in the germarium but not germline cells. We found that *Robo3, vnd, twist* and *bap* RNAs were absent from both cell populations, however, we found that *dpp*, *egfr* and *Stat92E* were equally present in GFP+ and RFP+ cells (Figure 1E and Table S1-2). These results indicated that there was no contamination by neural or mesodermal tissues, but that some ovarian somatic cells were equally present in both isolated cell populations. Despite the presence of somatic cells in both samples, our control experiments demonstrated that we were able to separate germline mitotic cells from meiotic cells, and that our results were consistent with previously published data.

We then took advantage of these transcriptome datasets to focus on genes required for the initial stages of meiosis I. We used the single GO term “meiosis I” in Flybase and removed male-specific genes to identify 69 genes. We found that all of these genes were expressed in both mitotic and meiotic cell populations (Figure 1E, Table S1-2). As previously shown by antibody staining, the synaptonemal complex components C(3)G, Corona and Ord were all found expressed in the mitotic region. We used the DESeq2 package to analyze the differential expression between these genes in the mitotic and meiotic cell populations. Except for a few exceptions, we found that most meiotic genes were expressed at low levels in region 1, and that their expression increase on average by 1.56 folds in region 2 (Figure 1E, Table S1). At one end, *hdm* expression is downregulated 2.3 folds from mitosis to meiosis, almost as strongly as our control gene *bam*, which expression is decreased by 2.7 folds (Figure 1E, Table S1). At the other end, the expression of *cortex* is increased by 4.1 folds. Genes encoding proteins required for homologous recombination such as *mei-W68* and *mei-P22* were among the least expressed in both cell types; nevertheless, their expression increased by 1.5 and 1.6 folds respectively in region 2.

To further validate our results, we performed a highly sensitive in situ hybridization (FISH) using the Hybridization Chain Reaction (HCR) method for *C(3)G*, *Nipped-B* and *mei-W68* RNAs (CHOI *et al.* 2018). To unambiguously distinguish the different stages within the mitotic and meiotic regions (Figure 2, yellow dotted line), we labeled the fusome with an antibody against α-Spectrin (Figure S2A-B). Consistent with our RNAseq data, we found that all three genes were expressed in region 1 cells; at very low levels for *mei-W68* and higher levels for *C(3)G* and *Nipped-B* (Figure 2A, C, E). Quantification of the fluorescent signals also revealed an increase in RNA levels for all three genes as found by the RNAseq analysis (Figure 2B, D, F).

Overall, we concluded that we were able to isolate the mitotic germline cells from the meiotic cells, and that all meiotic genes started to be expressed in mitotic cells.

2. *mei-W68* gene is expressed in the mitotic region but Mei-W68 protein is only detected in meiotic cells.

Spo11 and TopoVIBL form a meiosis-specific complex, which is conserved across species. In *Drosophila*, Mei-W68 is the homologue of Spo11, while Mei-P22 is a potential homologue of TopoVIBL (ROBERT *et al.* 2016; VRIELYNCK *et al.* 2016). The conserved function of this complex is to generate DSBs to initiate recombination between homologous chromosomes. However, in some species such as mouse, zebrafish, and recently jellyfish, these DSBs are also required for the formation of a SC (ROMANIENKO AND CAMERINI-OTERO 2000; BLOKHINA *et al.* 2019; MUNRO *et al.* 2023), whereas it is not the case in *C. elegans* and *Drosophila* females (DERNBURG *et al.* 1998; MCKIM *et al.* 1998). Here, we wanted to test whether Mei-W68 played a role in homologous chromosome pairing in region 1 before the initiation of meiotic DSBs.

As shown above using RNAseq and RNA FISH, we found that *mei-W68* mRNA is present at low levels in region 1. Next, we wanted to examine whether Mei-W68 protein was present in region 1. Since there is no antibody against Mei-W68 available in *Drosophila* and that Spo11 homologues are also very hard to detect in other species, we decided to knock-in a small 3xHA-6xHis tag by CRISPR-Cas9 at the C-terminus of the endogenous protein (Figure S4C). Despite successful integration, we found that the fusion protein was not functional, as no DSBs could be detected with an anti-γH2Av antibody in mei-W68-HA flies (Figure S5). Furthermore, we

found that the frequencies of X and chromosome II non-disjunction were similar in *mei-W68-HA/Df(*BSC782*)* and *mei-W68^{1}/Df(*BSC782*)* (Table S6A, S6B). However, *mei-W68-HA* RNAs were nonetheless translated as we were able to detect a specific signal in region 2a using an anti-HA antibody (Figure 3B). Quantification of this signal revealed that the levels of Mei-W68-HA protein in region 1 were at background levels, and dramatically increased in meiotic cells (Figure 3A', B', C). These results showed that Mei-W68 protein is probably not present in region 1, and that *mei-W68* mRNA is translated only in *Drosophila* meiotic cells.

3. Mei-W68 and Mei-P22 are dispensable for centromere pairing in the mitotic region.

The failure to detect Mei-W68 protein in the mitotic region could be due to limitations in our detection methods combined with its low expression levels, as suggested by our transcriptome analysis. We therefore used a functional assay to test for a requirement of Mei-W68 in region 1. In mouse germline cells, Spo11 has been proposed to be required for pre-meiotic pairing of homologous chromosomes (BOATENG *et al.* 2013). We thus assayed whether Mei-W68 was required for pre-meiotic pairing of centromeres in region 1. To this aim, we used three different mutant conditions. Firstly, in *mei-W68^{1}/DfBSC782* mutant germaria, there is a 5kb insertion of a transposable element in the first exon, and there is likely no protein made (MCKIM AND HAYASHI-HAGIHARA 1998) (Figure S4A). Secondly, we replaced by CRISPR-Cas9 the endogenous locus with a form of *mei-W68* mutated in the catalytic domain. Based on sequence alignment of similar constructs in yeast and mouse, we replaced two Tyrosine (Y80 and Y81) by two Phenylalanine in the catalytic domain (*mei-W68^{CD}* Figure S4B) (DIAZ *et al.* 2002; BOATENG *et al.* 2013). In this mutant background (*mei-W68^{1}/DfBSC782* and *mei-W68^{CD}*) no DSBs could be detected with an anti-γH2Av antibody (Figure S6A, S6B, S6C). Furthermore, we found high levels of non-disjunction for both the X and second chromosomes (Table S6A, S6B), indicating that *mei-W68^{CD}* is a strong mutant allele of *mei-W68.* Thirdly, we used a *mei-P22^{P22}* mutant allele and confirmed that DSBs were also completely absent (Figure S6D).

In previous studies, we observed that centromere pairing became prominent in 8-cell germline cysts (CHRISTOPHOROU N 2013). *Drosophila* diploid cells have four pairs of homologous chromosomes, resulting in eight chromosomes per cell. When all homologues are paired, we can observe four distinct dots of CID (Centromere Identifier) corresponding to

centromere pairing (TAKEO *et al.* 2011; TANNETI *et al.* 2011). However, when centromeres are not all paired, we can count more than four dots. In the nuclei of *mei-W68*$^{1/DfBSC782}$, *mei-W68*^{CD} and *mei-P22*^{P22} 8-cell cysts, we counted an average of 4.2, 4.4 and 4.2 ± 0.9-1.1, respectively, of CID foci as compared to 4.2 ± 0.9 in the wild-type (Figure 4 A-E), indicating that most chromosomes were paired at their centromeres in these three independent mutant conditions compared to wild type germaria (two-tailed Student's t-test, p=1 for *mei-W68*$^{1/DfBSC782}$; p=0.7 for *mei-W68*^{CD}; and p=0.8 for *mei-P22*^{P22}).

We also examined the pairing behavior of individual chromosomes in order to determine if pre-meiotic centromere pairing occurred between homologous chromosomes. To label the pericentromeric regions of chromosome II and III, we used the AACAC and dodeca probes respectively (JOYCE *et al.* 2012). To visualize pairing, we performed fluorescence *in situ* hybridization (DNA FISH) in combination with immunostaining against the fusome marker, α-Spectrin (Figure 4F-O). We defined chromosomes as paired when only one focus was detected or when two foci were detected with a separation distance of less than or equal to 0.70 µm (GONG WJ 2005; BLUMENSTIEL JP 2008). We found that in *mei-W68*$^{1/DfBSC782}$, *mei-W68*^{CD} and *mei-P22*^{P22} mutant 8-cell cysts, the number of paired chromosomes II at the level of the centromeric regions varies from 52.5% (wt) to 46.7% (*mei-W68*$^{1/DfBSC782}$; khi^2, p=0.5), 61.4% (*mei-W68*^{CD}; khi^2, p=0.3) and 35.4% (*mei-P22*^{P22}; khi^2, p=0.07) (Figure 4F-J); and for chromosome III, pairing varies from 57.4%, (wt) to 57.4%, (*mei-W68*$^{1/DfBSC782}$; khi^2 , p=1), 64.4% (*mei-W68*^{CD}; khi^2, p=0.4) and 60.8% (*mei-P22*^{P22}; khi^2, p=0.7) (Figure 4K-O). These results indicate that homologous chromosomes II and III were paired at their centromeres in all mutant conditions similarly to the wild type condition.

From these results, we concluded that Mei-W68 and Mei-P22 are not required for early centromere pairing.

4. Sunn, C(2)M, Nipped-B and Stromalin are dispensable for centromere pairing in the mitotic region

We previously showed that SC proteins C(3)G and Corona were expressed and required for centromere pairing in region 1 (CHRISTOPHOROU N 2013). Here, the RNAseq data indicated that many more SC or chromosome-axis proteins could be present in region 1, such as Sunn, C(2)M, Nipped-B or Stromalin (SA), which are meiotic cohesin or cohesin-associated proteins (HUGHES *et al.* 2018). To test whether these genes were required for centromere pairing in

region 1, we expressed shRNAs targeting each of these genes in germline cells (Figure 5). On average, we found that the numbers of centromere foci were similar between control germarium (sh-*white*) and in germarium mutant for *sunn*, *C(2)M*, *Nipped-B* and *Stromalin*, indicating that these genes are not required for the early pairing and clustering of centromeres (Figure 5A-F). We further tested the efficiency of these shRNA lines by estimating the frequencies of X-chromosome non-disjunction. We found that these lines induced efficiently between 8% and 14% of NDJ (Table S7). We concluded that, in contrast to SC proteins (C(3)G, Corona, Ord), cohesins associated to meiotic chromosomes were not required for centromere pairing.

5. DSBs activity is not detected in the premeiotic region

We then investigated whether DSBs could be present in region 1 despite the absence of Mei-W68 activity. In the *Drosophila* germline, the first sign of DSBs were described in region 2a using an antibody recognizing the phosphorylated H2A variant, also known as γH2Av (MEHROTRA AND MCKIM 2006; LAKE *et al.* 2013). To avoid using an antibody, we tested a GFP-tagged RPA transgene to label DSBs. RPA binds and protects single-strand DNA (ssDNA) just after resection of the double strand break. It is one the earliest known event of DSB repair. The coating of ssDNA by RPA is, however, transient as it is replaced by Rad51 filaments for DNA repair. To compare the pattern of DSBs precisely in the premeiotic and meiotic regions, we labeled the germarium with an antibody against α-spectrin recognizing 8cc stages, and against C(3)G to identify meiotic cells. In meiotic cysts, we selected the two pro-oocytes that displayed the brightest synaptonemal complex and counted their RPA::GFP dots in the early and late regions 2a and in region 2b (HUYNH AND ST JOHNSTON 2000; PAGE AND HAWLEY 2001). In a wild type germarium because RPA is rapidly replaced by Rad51, the GFP signal is expected to be very rare (Figure 6). Indeed, in this genetic context (*RpA-70::GFP*), we counted an average of 0 (8 cc), 0.7 (early 2a), 2.2 (late 2a) and 0.4 (region 2b) ±0.6-1.7 GFP foci (Figure 6 A, A', C, D, D', G, G', Movie S1). Furthermore, we found that most RPA-GFP foci were associated with γH2Av, while the opposite was not (Figure S7A, S7B, S7E), indicating a rapid replacement of RPA at DSBs sites.

We then introduced RpA-70 EGFP into a *spn-D* mutant background (*RpA-70::GFP, spn-D*^{2}). Spn-D is a meiosis-specific Rad51 homologue that is involved in removing and replacing RPA for DSBs repair in germline cells (ABDU *et al.* 2003). In this genetic context, we observed

accumulation of GFP dots in the meiotic region (Figure 6B, B', Movie S2) and not in the mitotic zone, counting an average of 0.2 (8 cc), 19 (early 2a), 16.7 (late 2a), 19.7 (2b pro-oocytes) ±0.4-4.4 GFP foci (Figure 6B, B', C, E, E', H, H'), respectively. We rarely detected RPA::GFP dots in the premeiotic region, indicating that neither Mei-W68 nor other sources induced detectable DSBs in the premeiotic region. In addition, we observed a much greater overlap between RPA and γH2Av dots in the *spn-D* mutant background than in the wild type condition (Figure S7C, S7D, S7E). This result confirmed the conserved role of Spn-D in RPA replacement during meiotic DSBs repair. Finally, in the additional absence of Mei-W68 (*mei-W68*$^{1/DfBSC782}$; *RpA-70::GFP*, *spn-D*^{2}), we counted 0 (8 cc), 0.2 (early 2a) and 0.3 (late 2a) ±0.3-0.4 GFP foci (Figure 6C, F, F', I, I'), indicating that Mei-W68 is responsible for most RPA dots in a *spn-D* mutant background, and importantly, that its activity is restricted to the meiotic region.

Discussion

In this work, we explored the transcriptome of known meiotic genes at a key transition of germline cell differentiation in *Drosophila* females. For this purpose, we used non-overlapping mitotic and meiotic cell populations genetically labelled with fluorescence transgenes in an otherwise completely wild type genetic background. Published methods for separating GSCs and differentiating cysts are based on the enrichment of GSCs in *bam* mutant conditions, and on the controlled expression of *bam* (*bam*RNAi; hs-*bam*) to enrich in differentiating cysts (KAI *et al.* 2005; WILCOCKSON AND ASHE 2019; MCCARTHY *et al.* 2022; SAMUELS *et al.* 2024). Wild type ovaries have been used for single cell technology assigning differentiation stages with known markers to cell clusters (JEVITT *et al.* 2020; SLAIDINA *et al.* 2021). These methods have provided vast resources for functional analyses. However, they have limitations in resolving with precision the distinct stages of mitosis and meiosis: the first produces mixed population of cysts, the second generated very few cell clusters, but has expanded up to nine distinct states. Our resulting transcriptome datasets reveal that in *Drosophila*, all the genes involved in the first stages of meiosis are already expressed at low levels in the dividing germ cells before they enter the meiotic prophase I. Importantly, we were able to recover from the RNA-seq datasets known meiotic genes expressed in the mitotic compartment confirming and extending our previous findings to the whole *Drosophila* genome (CHRISTOPHOROU N 2013).

Among these genes, we confirmed by in situ hybridization that *mei-W68* is transcribed in the premeiotic region showing increasing levels in the meiotic region. These results are in agreement with previous single cell transcriptome datasets in *Drosophila* ovaries, in which

germ cells in the germarium were staged using pseudotime analyses (SLAIDINA *et al.* 2021). Our study also provides new insights into the regulation of *mei-W68* in the germline. We inserted a small HA-His tag at the endogenous C-terminus of Mei-W68 and, although this construct is not fully functional, it allowed us to follow the pattern of *mei-W68* RNA translation. We found that Mei-W68 protein is detected mostly in early region 2a where meiotic DSBs localized and never in region 1. Thus, the primary factors contributing to the presence of Mei-W68 protein in the meiotic region are linked to the regulation of its translation. The importance of translational regulation during germ cell differentiation is well-known (SLAIDINA AND LEHMANN 2014; TEIXEIRA AND LEHMANN 2019). Recently, it has been quantified genomewide using Ribo-seq, and this study showed that it is hard to predict the amount of any proteins from the corresponding mRNA levels (SAMUELS *et al.* 2024). Nonetheless, the presence of meiotic mRNAs in germline mitotic cells may allow a faster transition to meiosis than the activation of meiotic transcription program at the onset of meiosis.

Interestingly, in the mouse, the role of SPO11 in the initiation of pairing was recently challenged. Two independent studies found that early pairing occurred at the premeiotic stage (BOATENG *et al.* 2013; SOLE *et al.* 2022), while two others detected pairing at early leptotene (ISHIGURO *et al.* 2014; SCHERTHAN *et al.* 2014); however, they all agreed that early pairing events were independent of DSBs. Moreover, Boateng and colleagues further showed that pairing was dependent on SPO11 but not of its catalytic activity (BOATENG *et al.* 2013). On the other hand, two independent labs found that SPO11 was not required at all for pairing (ISHIGURO *et al.* 2014; SCHERTHAN *et al.* 2014). These conflicting findings led us to ask for the requirement of Mei-W68 in premeiotic pairing in *Drosophila*. Here we show that neither Mei-W68 nor its putative partner Mei-P22 are involved in centromere pairing in the mitotic region of *Drosophila* females.

We used an Rpa70-GFP reporter as a new read-out of the initiation of meiotic recombination by DSBs (BLYTHE AND WIESCHAUS 2015). Phosphorylation of the histone variant H2Av (H2AX in mammals) is a widely-used mark for DSBs (MADIGAN *et al.* 2002). We found that in wild-type germarium, the timing and repair of meiotic DSBs reported previously using antibodies against γ-H2Av are in agreement with our results with Rpa70-GFP. RPA foci first appeared in early region 2a, peaked in late region 2a, and then declined in 2b (MEHROTRA AND MCKIM 2006; LAKE *et al.* 2013). The number of detectable RPA foci at any one time is, however, much smaller than with γ-H2Av, confirming that RPA coating of ssDNA is very transient (YADAV AND

CLAEYS BOUUAERT 2021). In contrast, in mutant conditions where DSBs are stabilized, we counted similar number of foci (19.7 in *spn-D* mutant region 2b) as previously published using antibody staining, 21.2 foci in *spn-D* mutant region 3 (MEHROTRA AND MCKIM 2006) and 19.3 foci in *okra* mutant region 2b (LAKE *et al.* 2013). As expected, in a *mei-W68* null background, no or few Rpa70-GFP foci were detected as previously reported using the γ-H2Av antibody (MEHROTRA AND MCKIM 2006; LAKE *et al.* 2013). Importantly, our results with fluorescently labeled Rpa70 confirmed that Mei-W68 does not exhibit early DSB activity in cysts before entering meiosis in region 2. Finally, our results also showed that there is no significant DSBs in the premeiotic region. In dividing embryos, the transient and rapid binding of Rpa70-GFP to sites of replication stress has allowed to measure optically the dynamics of stalled DNA replication during the mitotic cell cycle (BLYTHE AND WIESCHAUS 2015). Taking advantage of the properties of this reporter, we aim to follow by live imaging the *Drosophila* germarium events of initiation and repair of DSBs in the different genetic contexts.

Data availability statement

All fly strains are available upon request. Datasets are available from NCBI Sequence Reach Archive (SRA) under BioProject: PRJNA1011850 entitled “Isolation of stage-specific germ cells in *Drosophila* germarium”.

Acknowledgments

We are grateful to Shelby Blythe (U. Northwestern), Bloomington Stock Center, DSHB Hybridoma Center, for antibodies and flies. We are grateful to the Orion Imaging facility at CIRB (Collège de France).

JRH lab is supported by CNRS, Inserm, Collège de France, FRM (Equipe FRM DEQ20160334884); ANR ANR-20-CE12-, BioPic) and the Bettencourt-Schueller foundation (FBS).

Literature cited

Abdu, U., A. Gonzalez-Reyes, A. Ghabrial and T. Schupbach, 2003 The Drosophila spn-D gene encodes a RAD51C-like protein that is required exclusively during meiosis. Genetics 165**:** 197-204.

Bhalla, N., and A. F. Dernburg, 2008 Prelude to a division. Annu Rev Cell Dev Biol 24**:** 397-424.

Blokhina, Y. P., A. D. Nguyen, B. W. Draper and S. M. Burgess, 2019 The telomere bouquet is a hub where meiotic double-strand breaks, synapsis, and stable homolog juxtaposition are coordinated in the zebrafish, Danio rerio. PLoS Genet 15**:** e1007730.

Blumenstiel JP, F. R., Theurkauf WE, Hawley RS., 2008 Components of the RNAi machinery that mediate long-distance chromosomal associations are dispensable for meiotic and early somatic homolog pairing in Drosophila melanogaster. Genetics 180**:** 1355-1365.

Blythe, S. A., and E. F. Wieschaus, 2015 Zygotic genome activation triggers the DNA replication checkpoint at the midblastula transition. Cell 160**:** 1169-1181.

Boateng, K. A., M. A. Bellani, I. V. Gregoretti, F. Pratto and R. D. Camerini-Otero, 2013 Homologous pairing preceding SPO11-mediated double-strand breaks in mice. Dev Cell 24**:** 196-205.

Cahoon, C. K., and R. S. Hawley, 2013 Flies get a head start on meiosis. PLoS Genet 9**:** e1004051.

Cahoon, C. K., and R. S. Hawley, 2016 Regulating the construction and demolition of the synaptonemal complex. Nat Struct Mol Biol 23**:** 369-377.

Carpenter, A. T., 1975 Electron microscopy of meiosis in Drosophila melanogaster females. I. Structure, arrangement, and temporal change of the synaptonemal complex in wild-type. Chromosoma 51**:** 157-182.

Chen, D., and D. M. McKearin, 2003 A discrete transcriptional silencer in the bam gene determines asymmetric division of the Drosophila germline stem cell. Development 130**:** 1159-1170.

Choi, H. M. T., M. Schwarzkopf, M. E. Fornace, A. Acharya, G. Artavanis *et al.*, 2018 Third-generation in situ hybridization chain reaction: multiplexed, quantitative, sensitive, versatile, robust. Development 145.

Christophorou N, R. T., Huynh JR., 2013 Synaptonemal complex components promote centromere pairing in pre-meiotic germ cells. PLoS Genet 9**:** e1004012.

Christophorou, N., T. Rubin, I. Bonnet, T. Piolot, M. Arnaud *et al.*, 2015 Microtubule-driven nuclear rotations promote meiotic chromosome dynamics. Nat Cell Biol 17**:** 1388-1400.

Cinalli, R. M., P. Rangan and R. Lehmann, 2008 Germ cells are forever. Cell 132**:** 559-562.

Crittenden SL, L. K., Byrd DT, Kimble J., 2006 Cellular Analyses of the Mitotic Region in the Caenorhabditis elegans Adult Germ Line. Molecular Biology of the Cell.

de Cuevas, M., and A. C. Spradling, 1998 Morphogenesis of the Drosophila fusome and its implications for oocyte specification. Development 125**:** 2781-2789.

de Massy, B., 2013 Initiation of meiotic recombination: how and where? Conservation and specificities among eukaryotes. Annu Rev Genet 47**:** 563-599.

Dernburg, A. F., K. McDonald, G. Moulder, R. Barstead, M. Dresser *et al.*, 1998 Meiotic recombination in C. elegans initiates by a conserved mechanism and is dispensable for homologous chromosome synapsis. Cell 94**:** 387-398.

Diaz, R. L., A. D. Alcid, J. M. Berger and S. Keeney, 2002 Identification of residues in yeast Spo11p critical for meiotic DNA double-strand break formation. Mol Cell Biol 22**:** 1106-1115.

Dufourt, J., C. Dennis, A. Boivin, N. Gueguen, E. Theron *et al.*, 2014 Spatio-temporal requirements for transposable element piRNA-mediated silencing during Drosophila oogenesis. Nucleic Acids Res 42**:** 2512-2524.

Evans, E., C. Hogarth, D. Mitchell and M. Griswold, 2014 Riding the spermatogenic wave: profiling gene expression within neonatal germ and sertoli cells during a synchronized initial wave of spermatogenesis in mice. Biol Reprod 90**:** 108.

Fang, K., Q. Li, Y. Wei, C. Zhou, W. Guo *et al.*, 2021 Prediction and Validation of Mouse Meiosis-Essential Genes Based on Spermatogenesis Proteome Dynamics. Mol Cell Proteomics 20**:** 100014.

Fichelson, P., C. Moch, K. Ivanovitch, C. Martin, C. M. Sidor *et al.*, 2009 Live-imaging of single stem cells within their niche reveals that a U3snoRNP component segregates asymmetrically and is required for self-renewal in Drosophila. Nat Cell Biol 11**:** 685-693.

Gong WJ, M. K., Hawley RS., 2005 All paired up with no place to go: pairing, synapsis, and DSB formation in a balancer heterozygote. PLoS Genet 1**:** e67.

Gyuricza, M. R., K. B. Manheimer, V. Apte, B. Krishnan, E. F. Joyce *et al.*, 2016 Dynamic and Stable Cohesins Regulate Synaptonemal Complex Assembly and Chromosome Segregation. Curr Biol.

Hughes, S. E., D. E. Miller, A. L. Miller and R. S. Hawley, 2018 Female Meiosis: Synapsis, Recombination, and Segregation inDrosophila melanogaster. Genetics 208**:** 875-908.

Huynh, J. R., and D. St Johnston, 2000 The role of BicD, Egl, Orb and the microtubules in the restriction of meiosis to the Drosophila oocyte. Development 127**:** 2785-2794.

Huynh, J. R., and D. St Johnston, 2004 The origin of asymmetry: early polarisation of the Drosophila germline cyst and oocyte. Curr Biol 14**:** R438-449.

Ishiguro, K., J. Kim, H. Shibuya, A. Hernandez-Hernandez, A. Suzuki *et al.*, 2014 Meiosis-specific cohesin mediates homolog recognition in mouse spermatocytes. Genes Dev 28**:** 594-607.

Jevitt, A., D. Chatterjee, G. Xie, X. F. Wang, T. Otwell *et al.*, 2020 A single-cell atlas of adult Drosophila ovary identifies transcriptional programs and somatic cell lineage regulating oogenesis. PLoS Biol 18**:** e3000538.

Joyce EF, A. N., Beliveau BJ, Wu CT., 2013 Germline progenitors escape the widespread phenomenon of homolog pairing during Drosophila development. PLoS Genet 9**:** e1004013.

Joyce, E. F., B. R. Williams, T. Xie and C. T. Wu, 2012 Identification of genes that promote or antagonize somatic homolog pairing using a high-throughput FISH-based screen. PLoS Genet 8**:** e1002667.

Kai, T., D. Williams and A. C. Spradling, 2005 The expression profile of purified Drosophila germline stem cells. Dev Biol 283**:** 486-502.

Keeney, S., C. N. Giroux and N. Kleckner, 1997 Meiosis-specific DNA double-strand breaks are catalyzed by Spo11, a member of a widely conserved protein family. Cell 88: 375-384.

Kim, H. J., C. Liu and A. F. Dernburg, 2022 How and Why Chromosomes Interact with the Cytoskeleton during Meiosis. Genes (Basel) 13.

Lake, C. M., J. K. Holsclaw, S. P. Bellendir, J. Sekelsky and R. S. Hawley, 2013 The development of a monoclonal antibody recognizing the Drosophila melanogaster phosphorylated histone H2A variant (gamma-H2AV). G3 (Bethesda) 3: 1539-1543.

Madigan, J. P., H. L. Chotkowski and R. L. Glaser, 2002 DNA double-strand break-induced phosphorylation of Drosophila histone variant H2Av helps prevent radiation-induced apoptosis. Nucleic Acids Res 30: 3698-3705.

McCarthy, A., K. Sarkar, E. T. Martin, M. Upadhyay, S. Jang *et al.*, 2022 Msl3 promotes germline stem cell differentiation in female Drosophila. Development 149.

McKearin, D., and B. Ohlstein, 1995 A role for the Drosophila bag-of-marbles protein in the differentiation of cystoblasts from germline stem cells. Development 121: 2937-2947.

McKim, K. S., B. L. Green-Marroquin, J. J. Sekelsky, G. Chin, C. Steinberg *et al.*, 1998 Meiotic synapsis in the absence of recombination. Science 279: 876-878.

McKim, K. S., and A. Hayashi-Hagihara, 1998 mei-W68 in Drosophila melanogaster encodes a Spo11 homolog: evidence that the mechanism for initiating meiotic recombination is conserved. Genes & Development 12: 2932-2942.

Mehrotra, S., and K. S. McKim, 2006 Temporal analysis of meiotic DNA double-strand break formation and repair in Drosophila females. PLoS Genet 2: e200.

Munro, C., H. Cadis, S. Pagnotta, E. Houliston and J. R. Huynh, 2023 Conserved meiotic mechanisms in the cnidarian Clytia hemisphaerica revealed by Spo11 knockout. Sci Adv 9: eadd2873.

Page, S. L., and R. S. Hawley, 2001 c(3)G encodes a Drosophila synaptonemal complex protein. Genes Dev 15: 3130-3143.

Pasierbek, P., M. Jantsch, M. Melcher, A. Schleiffer, D. Schweizer *et al.*, 2001 A Caenorhabditis elegans cohesion protein with functions in meiotic chromosome pairing and disjunction. Genes Dev 15: 1349-1360.

Robert, T., A. Nore, C. Brun, C. Maffre, B. Crimi *et al.*, 2016 The TopoVIB-Like protein family is required for meiotic DNA double-strand break formation. Science 351: 943-949.

Rohozkova, J., L. Hulkova, J. Fukalova, P. Flachs and P. Hozak, 2019 Pairing of homologous chromosomes in C. elegans meiosis requires DEB-1 - an orthologue of mammalian vinculin. Nucleus 10: 93-115.

Romanienko, P. J., and R. D. Camerini-Otero, 1999 Cloning, characterization, and localization of mouse and human SPO11. Genomics 61: 156-169.

Romanienko, P. J., and R. D. Camerini-Otero, 2000 The Mouse Spo11 Gene Is Required for Meiotic Chromosome Synapsis. Molecular Cell 6: 975-987.

Rubin, T., N. Macaisne and J. R. Huynh, 2020 Mixing and Matching Chromosomes during Female Meiosis. Cells 9.

Rubin, T., N. Macaisne, A. M. Valles, C. Guilleman, I. Gaugue *et al.*, 2022 Premeiotic pairing of homologous chromosomes during Drosophila male meiosis. Proc Natl Acad Sci U S A 119: e2207660119.

Samuels, T. J., J. Gui, D. Gebert and F. Karam Teixeira, 2024 Two distinct waves of transcriptome and translatome changes drive Drosophila germline stem cell differentiation. EMBO J.

Scherthan, H., K. Schofisch, T. Dell and D. Illner, 2014 Contrasting behavior of heterochromatic and euchromatic chromosome portions and pericentric genome separation in pre-bouquet spermatocytes of hybrid mice. Chromosoma 123: 609-624.

Slaidina, M., S. Gupta, T. U. Banisch and R. Lehmann, 2021 A single-cell atlas reveals unanticipated cell type complexity in Drosophila ovaries. Genome Res 31**:** 1938-1951.

Slaidina, M., and R. Lehmann, 2014 Translational control in germline stem cell development. J Cell Biol 207**:** 13-21.

Sole, M., J. Blanco, D. Gil, O. Valero, B. Cardenas *et al.*, 2022 Time to match; when do homologous chromosomes become closer? Chromosoma.

Spradling, A. C., 1993 Developmental genetics of oogenesis. 1--70.

Takeo, S., C. M. Lake, E. Morais-de-Sa, C. E. Sunkel and R. S. Hawley, 2011 Synaptonemal complex-dependent centromeric clustering and the initiation of synapsis in Drosophila oocytes. Curr Biol 21**:** 1845-1851.

Tanneti, N. S., K. Landy, E. F. Joyce and K. S. McKim, 2011 A pathway for synapsis initiation during zygotene in Drosophila oocytes. Curr Biol 21**:** 1852-1857.

Teixeira, F. K., and R. Lehmann, 2019 Translational Control during Developmental Transitions. Cold Spring Harb Perspect Biol 11.

Tsubouchi T, R. G., 2005 A synaptonemal complex protein promotes homology-independent centromere coupling. Science 308**:** 870-873.

Valles, A. M., and J. R. Huynh, 2020 Isolation of stage-specific germ cells using FACS in Drosophila germarium. Methods Cell Biol 158**:** 11-24.

Vrielynck, N., A. Chambon, D. Vezon, L. Pereira, L. Chelysheva *et al.*, 2016 A DNA topoisomerase VI–like complex initiates meiotic recombination. Science 351**:** 939-941.

Wang, P. J., J. R. McCarrey, F. Yang and D. C. Page, 2001 An abundance of X-linked genes expressed in spermatogonia. Nat Genet 27**:** 422-426.

Wilcockson, S. G., and H. L. Ashe, 2019 Drosophila Ovarian Germline Stem Cell Cytocensor Projections Dynamically Receive and Attenuate BMP Signaling. Dev Cell 50**:** 296-312 e295.

Yadav, V. K., and C. Claeys Bouuaert, 2021 Mechanism and Control of Meiotic DNA Double-Strand Break Formation in S. cerevisiae. Front Cell Dev Biol 9**:** 642737.

Zheng, Y., L. Zhang, L. Jin, P. Zhang, F. Li *et al.*, 2022 Unraveling three-dimensional chromatin structural dynamics during spermatogonial differentiation. J Biol Chem 298**:** 101559.

Zickler, D., and N. Kleckner, 2015 Recombination, Pairing, and Synapsis of Homologs during Meiosis. Cold Spring Harb Perspect Biol 7.

MATERIAL AND METHODS

Flies were maintained on standard medium in 25°C incubators on a 12 h light/dark cycle. Wild-type controls and in combination with additional transgenes of fluorescently tagged proteins were in a w^{1118} background.

Fly stocks and genetics

Fly stocks used in this study: *bam::GFP/CyO; nos>UASp-RFP::wcd/TM6,tb,* is the full-length *bam* fused to GFP at C-terminus, containing its own promoter and 3'UTR (CHEN AND MCKEARIN 2003) and full-length *wicked* fused to RFP N-terminus, under the control of germline specific UASp promoter and activated by *nanos-Gal::VP16* (BDSC_4937) (FICHELSON *et al.* 2009). To compare *bam::GFP/CyO; nos>UASp-RFP::wcd/TM6,tb* line to the wild type white- reference line, we first used Orb as a marker for developmental timing of germline development (Figure S1A, S1B). We found no difference between the bam-Bam::GFP; nos>wcd::RFP line and the white- control line. Orb is initially present in all germline cells in early region 1 and 2a, then becomes restricted to the oocyte in region 2b, at the anterior of the oocyte in region 3 and then switches to the posterior of the oocyte in stage 2 egg chambers. We found the two lines to be identical. We also analyzed the restriction of the synaptonemal complex to a single cell using an antibody against C(3)G (Figure S1C and S1D). We found that in region 1 and region 2a, C(3)G was identical in both genetic backgrounds. However, in region 3, we noticed that the SC signal was less intense in the future oocyte in the transgenic line (Figure S1E, "oocyte I"); and at the same time, we observed a stronger signal of C(3)G in the reverting pro-oocyte in the transgenic line (Figure S1D, open arrowhead, Figure S1E, "oocyte II"). Then at stage 2, the transgenic and control lines became identical. These data indicate that there is a transient delay in the restriction of the SC to a single cell in the *bam-Bam::GFP; nos>wcd::RFP line* compared to white- flies. We then tested whether this delay could be caused by different number of germline cysts in the germarium, but we found no difference in number of cysts in region 2 between the two genetic backgrounds (Figure S1F). We also analyzed by RNA FISH whether we could detect differences in gene expression between the two lines. We performed RNA FISH for meiotic genes found in RNAseq data, such as *c(3)G*, *Nipped-B* and *mei-W68* (Figure S3A,B,C). Quantification of FISH signals in region 2 found no difference in levels of expression of these three genes between the transgenic and control line. Finally, we used a functional assay to test for meiotic differences between these two lines, and we measured the occurrence of X-chromosome non-disjunction (Table S5).

In both lines, we found only background frequencies of chromosome non-disjunctions. Overall, our thorough characterization of the *bam-Bam::GFP; nos>wcd::RFP* line revealed only a transient delay in SC restriction to the oocyte. This does not change our transcriptomic analysis of region 1 and 2.

mei-W68 ^{HA} is a C-terminal 3x HA-linker-6x His tagged *mei-W68* fly, homozygous viable and sub-fertile generated by CRISPR/Cas9 mediated Tag knocking strategy (Well Genetics). Catalytic dead *mei-W68* ^{CD} was genome edited at the conserved catalytic domain (Y80F, Y81F) (ROMANIENKO AND CAMERINI-OTERO 1999) using the seamless CRISPR/Cas9 strategy (Well Genetics). Flies are homozygous viable and sub-fertile. *mei-W68*^{1} is a null mutation caused by spontaneous 5kb TE insertion in exon 2, females have normal synaptonemal complex but show elevated NDJ levels (MCKIM AND HAYASHI-HAGIHARA 1998). Df (2R) BSC782/SM6a (BDSC_27354) is a *mei-W68* deficiency. *mei-P22*^{P22} (BDSC_4931). The shRNA lines were: for *white*, P{TRiP.GL00094}attP2 (BDSC_35573); for *C(2)M* P{TRiP.GL01587}attP2 (BDSC_43977); for *SA* P{TRiP.GL00534}attP40 (BDSC_36794), for *Nipped-B* P{ TRiP.GL00574}attP40 (BDSC_36614), for *sunn* P{TRiP.HMJ21654} (BDSC_52969). *spn-D*^{2} (BDSC_3326). *y w; RpA-70 EGFP[attP2]* (BLYTHE AND WIESCHAUS 2015) flies were used to generate lines: *Rpa-70 EGFP spn-D*^{2} , *mei-W68*^{1}/CyO ; *Rpa-70 EGFP spn-D*^{2}, *Df (2R)BSC782/CyO* ; *Rpa-70 EGFP spn-D*^{2} */TM6,tb.*

FACS sorted germ cells

We used the protocol for isolating mitotic and meiotic cell populations as detailed in Vallés and Huynh 2020. In brief, for each FACS isolation, 800 adult ovaries from *bam::GFP/CyO; nos>UASp-RFP::wcd/TM6,tb* flies were dissected and collected in complete medium (Schneider's insect medium supplemented with 10% heat-inactivated fetal bovine serum, Sigma-Aldrich), dissociated with elastase at 30°C for 30 min (1 mg/ml, Sigma-Aldrich), and filtered twice (first in 40µ mesh size, then in 70µ mesh size, Corning Falcon). Cell suspensions underwent FACS separation (Aria III, BD Biosciences), collecting GFP+ and RFP+ cells and eliminating non-fluorescent cells, clumps, and dead cells. Cells were sorted directly into RNA extraction buffer (ARCTURUS Pico RNA isolation Kit, Applied Biosystems) for purification following manufacturer's protocol.

Library preparations were done by Fasteris SA (Geneva, Switzerland) using the RNA RiboZero Stranded protocol. Indexed adapters were ligated and multiplexed sequencing performed using Illumina HiSeq 2000 (125-bp single read). At least two independent biological samples were prepared for each cell population. Sequences generated by Fasteris were aligned against the *D.*

melanogaster reference genome (UCSC dm6) http://rohsdb.cmb.usc.edu/GBshape/cgi-bin/hgGateway.

RT-qPCR

To validate FACS separations (Figure 1H), RFP+ and GFP+ sorted cells from *BAM::GFP; nos>Wcd::RFP* ovaries were homogenized with a pestle and RNA extracted using the ARCTURUS PicoPure RNA isolation kit.

To quantify gene expression in *mei-W68 ^{1}/ Df (2R) BSC782* flies (Figure S4B), RNA was extracted from 20 pairs of dissected ovaries using the RNeasy Micro Kit (QIAGEN). RNA from w^{1118}ovaries served as control.

For all RT-qPCR reactions, reverse transcription was done using random hexamer oligonucleotides with Superscript III Reverse Transcriptase (Invitrogen) according to manufacturer's protocol, then by RT- PCR using *Power* SYBR Green© PCR Master Mix (applied biosystems). Amplifications were done on a CFX Connect Real-Time PCR machine (Bio-Rad). Two to three biological replicates per genotype were used for all RT-qPCR experiments run in triplicate.

Relative expression levels of tested genes were calculated by the *C*t method with samples normalized to *rp49* (Schmittgen and Livak, 2008). For each experiment, primer expression in *mei-W68^{1}* was compared to w^{1118} equal 1. To compare gene expression levels between the two isolated cell populations, we first normalized each target sample (2-3) with the *C*t method (to *rp49)*. For each experiment, we then normalized the highest value of the two populations to 1. Expression values collected from 3-5 experiments were analyzed and transformed into graphs with Prism8 software. Mann-Whitney tests were applied to compare data.

The primers used for validation of isolated cell populations were:

GFP: F 5'AGAGGGCGAATCCAGCTCTGGAG 3', R 5'CCCAAATCGGCGGTCAGGTGATC 3';

RFP: F 5' GTCCCCTCAGTTCCAGTACG 30, R 5' TGTAGATGAACTCGCCGTC 3';

bam: F 5'CTGCATATGATTGGTCTGCACGGC 3', R 5'CCCAAATCGGCGGTCAGGTGATC 3';

piwi: F 5' CAGAGGATCTTCATCAGGTG 3', R 5' ATCATATTGGTCACCCCAC 3';

mtrm: F 5' GAAAGTGCCAACGAAGGTGC 3', R 5' CTCCATATTCGAGTCATCCGAAC 3';

The *mei-W68* primers were:

A: F 5' AGCTGCTGCTACTGCTGCTG 3', R 5' CCGACTTTTACCGAACGAAAACGAC 3';

B: F 5' GCTAGAACAATG GATGAATTTTCGG 3', R 5' GGAGAGCATGTAAAT CAGCACG 3';

C: F 5' CGTGCTGATTTACATGCTCTCC 3', R 5' GACCGGACTAGCAGAGGATT 3'.

rp49: F 5'ATCTCGCCGCAGTAAACGC 3', R 5'CCGCTTCAAGGGACAGTATCTG 3'.

Data analysis and heatmap generation

The DESeq2 method for differential analysis of RNA-seq data was used (Love et al 2014). As input, we used three GFP and two RFP distinct biological replicates with counts normalized for differences in sequencing depth using the DESeq normalization tool in Galaxy Mississipi[2] platform (https://mississippi.sorbonne-universite.fr). The normalized raw counts were then used to calculate the base mean for each gene expressed in the mitotic and meiotic cell population to generate the "DESeq2 results extended with basemeans of conditions" file (Table S3). Gene lengths were taken into account by calculating FPKM for each gene (Table S4). We then extracted a subset of genes (meiotic, somatic and separation controls) and obtained Table S1 (in FPKM Table S2) used for creating a heatmap (Figure 1E). To generate the heatmap, a list of meiotic genes was compiled from FlyBase GO term (GO: 0007127), excluding genes identified as male-specific and unannotated. Added to the list are known meiotic genes (*SMC1, SMC3, sunn, solo, ord*), *RpA-70, dpp, egfr, Stat9e,*sorting (*bam* and *wcd*), and contamination controls possibly derived from somatic tissues like gut, fat, introduced during dissection of ovaries (*robo3, vnd, bap, twi)* (See Table S1). The resulting values were transformed to log2 and used to generate a heatmap with the heatmap2 tool in the Galaxy Mississipi[2] platform.

Datasets repository

Datasets are available from NCBI Sequence Reach Archive (SRA) under BioProject: PRJNA1011850 entitled "Isolation of stage-specific germ cells in *Drosophila* germarium".

Nondisjunction Tests

Sex chromosome nondisjunction was monitored by scoring the progeny of *y/BS Y* males mated to females carrying meiotic mutations on the second or third chromosome. For crosses with RNAi lines, the *nanos-Gal::VP16* driver was used. In most cases, a male to female ratio of 5:10 was kept. From these crosses, exceptional diplo-X and nullo-X resulting from sex chromosome

nondisjunction and normal gametes are obtained. Frequency of *X* chromosome nondisjunction was calculated as 2(X-ND progeny)/total progeny, where total progeny =[2(X-ND progeny) + (regular progeny) (GYURICZA *et al.* 2016). To determine autosomal 2nd chromosome nondisjunction, females carrying meiotic mutations were mated to *C(2)EN b pr* (BDSC: 1112) males and the number of progeny scored. In most cases, a male to female ratio of 5:10 was kept. From these crosses, only the exceptional diplo-2 and nullo-2 gametes are observed.

Immunohistochemistry

For confocal microscopy, ovaries were dissected in PBS, fixed in 4% PFA–PBS, and then permeabilized in PBT (0.2% Triton) for 30 min. Samples were incubated overnight with primary antibodies in PBT at 4 °C, washed 4 × 30 min in PBT, incubated with secondary antibody for 2 h at room temperature, washed 4 × 30 min in PBT. DAPI (1:500) was added during the last wash and then mounted in CityFluor.

For DNA FISH experiments, ovaries were dissected in PBS, fixed in 4% PFA in 1X fix buffer (100 mm potassium cacodylate, 100 mm sucrose, 40 mm sodium acetate, and 10 mm EGTA). Samples were then rinsed three times in 2X SSCT and incubated with the AACAC and dodeca probes which target the pericentromeric regions of the 2nd and 3rd chromosomes, respectively, as previously described (CHRISTOPHOROU N 2013). Samples were then rinsed in 2X SSCT, twice in PBST and process for immunostaining as described above for confocal microscopy.

For RNA FISH experiments, we followed the HCR *in situ* hybridization protocol for ovaries as described in (SLAIDINA *et al.* 2021), which was adapted from (CHOI *et al.* 2018) Custom designed probes for *mei-W68* (NT_033778), hybridization buffer, wash buffer, and amplification buffer came from Molecular Instruments Inc.

The following primary antibodies were used: mouse anti-C(3)G 1A8-1G2 (1:500) (gift from S. Hawley, Stowers Institute, USA), rat anti-Cid (1:1,000) (gift from C. E. Sunkel, Universidade do Porto, Portugal), rabbit anti-α-Spectrin (1:1,000 and 1:500 when used with DNA FISH) (gift from R. Dubreuil, University of Chicago, USA), mouse anti-α-Spectrin (1:500, clone 3A9, DSHB), mouse anti-orb (1:500, clone 6H4, DSHB), mouse anti-γH2Av (1:200) (DSHB, UNC93-5.2.1), rabbit anti-HA-Tag (1:100) (Cell Signaling Technologies, C29A4).

Secondary antibodies conjugated with Cy3, Cy5, (Jackson laboratories) were used at 1:200, Alexa Fluor Plus 555, and 647 at 1:400 (Thermo Fisher Scientific).

Image acquisition

Ovaries for imaging were taken from 3-5 day-old flies. Confocal images of fixed germaria were obtained with a Zeiss LSM 980 NLO confocal microscope except for Supplementary Figure 1. All images were acquired with a PlanApo 63×/1.4 NA oil objective at 0.5 µm intervals along the z-axis operated by ZEN 2012 software. For supplementary Figure 1, confocal images of fixed germaria were taken with a spinning-disc confocal microscope (Yokogawa) operated by Metamorph software on an inverted Nikon Eclipse Ti microscope coupled to a Coolsnap HQ2 camera (Photometrics). All images were acquired with the PlanApo 60×/1.4 NA Oil objective.

Live imaging in oil

Ovaries were dissected in oil (10S, Voltalef, VWR) and transfer onto a coverslip. Germaria were made to stick to the coverslip in oil. All images were acquired on an inverted spinning-disc confocal microscope (Roper/Nikon) operated by Metamorph 7.7 coupled to an sCMOS camera and with a 60X/1.4 oil objective. 1 z-stack acquired every 30sec.

Data analysis of images

For quantification of CID foci on fixed tissue, we counted the number of distinguishable CID foci within each single nucleus. In all figures, micrographs represent the projections of selected z-series taken from the first CID foci signal until the last one. For DNA FISH experiments, the 3D distances between the AACAC foci and between the dodeca foci were measured as described (CHRISTOPHOROU N 2013). Pericentromeric regions of chromosomes were considered as paired when only one foci was visible or when two foci were separated by a distance less than 0.70 µm, and as unpaired when ≥ 0.70 µm.

Fluorescence intensity measurements of RNA FISH were performed on Z-stack images acquired with identical settings. To define a Region of Interest (ROI), a Z MAX projection of 3 successive images within a circle of 50 pixels in diameter was chosen at the center of each analyzed cyst. The cyst stage was determined using the spectrin channel. Cysts located in region 2 were considered as meiotic cysts, while branched cysts of 2-cc, 4-cc, and 8-cc were classified as mitotic cysts. As background control, the ROI was selected in the somatic cells of the nascent stalk before the region 3 cyst of each analyzed germarium. For each cyst and control ROI, the Raw Integrated Density was quantified using Fiji software. The raw data were then transformed into graphs with Prism8 software. Mann-Whitney tests were used to compare fluorescence intensity.

Fluorescence intensity measurements of C(3)G were performed on Z-stack images acquired with identical settings. To define a Region of Interest (ROI), a Z MAX projection of 3 successive images within a circle of 50 pixels in diameter was chosen at the center of the C(3)G marked nuclei. The cyst stage was determined using C(3)G staining location in the germarium. As background control, the ROI was selected in the somatic cells of the nascent stalk before the region 3 cyst of each analyzed germarium. For each cyst and control ROI, the Raw Integrated Density was quantified using Fiji software. The raw data were then transformed into graphs with Prism8 software. Mann-Whitney tests were used to compare fluorescence intensity.

Mean Cyst number estimation in meiotic region 2 were performed on Z-stack images acquired with identical settings. Cysts boundaries were defined thanks to α-Spectrin staining, and counted manually.

For the quantification of RPA and H2Av foci on fixed tissues, we counted the number of distinct foci within each individual nucleus. For each channel, the signal was processed using the difference of Gaussians tool available in the GDSC plugin for Fiji. Default Threshold was then applied to the resulting stack, generating binary images reconstructed into a three-dimensional stack using the 3D segmentation function of RoiManager3D 4.1.5. The counting of RPA and H2Av dots and the percentage of 'overlap' were then calculated using the 'Measure 3D' analysis.

Figure Legends

Figure 1. Meiotic genes are expressed in the mitotic region of the *Drosophila* germarium

(A) Drosophila germarium depicting the mitotic and meiotic regions. In the anterior part (Mitotic zone, also called region 1) at the base of the terminal filament (TF), somatic cap cells surround germline stem cells (GSC) that divide four times giving rise to a 16-cells cyst. GSCs and cystoblasts (CB) are marked by the spectrosome (red circle), and the developing two-, four, and eight-cell cysts by the fusome (red-branched structure). After the last mitosis, cysts move to the meiotic zone, subdivided in region 2a, 2b and 3. Early in region 2a, the synaptonemal complex (red thin lines) marks the pro-oocytes with four ring canals. By region 2b, the oocyte is selected and is the only cell (yellow) to remain in meiosis. The follicle cells (FC) start to migrate and surround the germline cells as the cyst moves posteriorly to region 3.

(B-B'') Confocal Z-section of a germarium labelling the mitotic region with Bam::GFP (Green), the meiotic region with Wcd::RFP (magenta), the synaptonemal complex with C(3)G (white) and cell nuclei with DAPI (blue). (C, C') Magnification of hatched square in B showing C(3)G nuclear labelling of a cell in the mitotic region (open arrows) adjacent to a synaptonemal complex labelled pro-oocyte. Scale bar: 10 µm in B-B'' 2 µm in C, C'.

(D) RT-PCR gene expression levels of FACS-separated mitotic (green) and meiotic (magenta) cells using primers to GFP, RFP, *bam*, *piwi* and *mtrm*. Gene expression levels are defined to 1 relative to the highest value within both population after rp49 normalization. * $p \leq 0.05$, ** $p \leq 0.01$, *** $p \leq 0.001$, **** $p \leq 0.0001$ (Mann-Whitney U-test)

(E) Heat map of known meiotic genes expressed in FACS-separated Bam::GFP (Mitotic) and Wcd::RFP cells (Meiotic). In the upper pannel are the somatic genes, *robo3, vnd* (neural); *bap, twi (*mesodermal); *dpp, Egfr, Stat92e* (follicle cells) and the sorting controls *bam, blanks, nos* and *wcd*. The middle and lower panels represent the heat map of meiotic genes. Scale represents log2 expression gradient for genes expressed in each of the two regions. Notice that neural and mesodermal contaminants are not detected while follicle cells ones are equally present in both cell populations.

Figure 2. *c(3)G*, *Nipped-B* and *mei-W68* meiotic genes mRNA are detected in the mitotic region and their levels increase in the meiotic region

(A) Confocal Z-section projection of a *WT* germarium labelled for *c(3)G* mRNA by HCR *in situ* hybridization. The yellow dashed line delimits the boundary of mitotic and meiotic regions.

Scale bar: 10 μm. (B) Graph plots *c(3)G mRNA* Fluorescence Intensity in mitotic and meiotic 2a regions. *** $p \leq 0.001$ (Mann-Whitney U-test).

(C) Confocal Z-section projection of a *WT* germarium labelled for *Nipped-B* mRNA by HCR *in situ* hybridization. The yellow dashed line delimits the boundary of mitotic and meiotic regions. Scale bar: 10 μm. (D) Graph plots *Nipped-B mRNA* Fluorescence Intensity in mitotic and meiotic 2a regions. ** $p \leq 0.01$ (Mann-Whitney U-test).

(E) Confocal Z-section projection of a *WT* germarium labelled for *mei-W68* mRNA by HCR *in situ* hybridization. The yellow dashed line delimits the boundary of mitotic and meiotic 2a regions. Scale bar: 10 μm. (F) Graph plots *mei-W68 mRNA* Fluorescence Intensity in mitotic and meiotic regions. * $p \leq 0.05$ (Mann-Whitney U-test). (*n*) is the number of germaria analyzed for each probe.

Figure 3. Mei-W68 protein is only detected in the meiotic region. (A-A') Confocal Z-section projection of a *WT* germarium immunostained for HA (green) and the fusome (magenta). The yellow dashed line delimits the boundary of mitotic and meiotic regions. Scale bar: 10 μm.

(B, B') Confocal Z-section projection of a $mei\text{-}W68^{HA}/+$ germarium immunostained for HA (green) and the fusome (magenta). The yellow dashed line delimits the boundary of mitotic and meiotic regions. Scale bar: 10 μm. Note that HA immunostaining is barely detectable in both regions (A, A') of *WT*, while HA is clearly confined to the meiotic region of $W68^{HA}/+$ (compare mitotic and meiotic region in in B, B').

(C) Graph plots HA Fluorescence Intensity in mitotic and meiotic regions. ns $p \geq 0.05$, *** $p \leq 0.001$, **** $p \leq 0.0001$ (Mann-Whitney U-test). Numbers below bars represent the germaria analysed.

Figure 4. *mei-W68* and *mei-P22* are dispensable for 8-cell cyst chromosome pairing in females.

A-E, Cid pairing in *mei-W68* and *mei-P22* mutant cysts. (A-D) Confocal Z-section projections of wild type (*WT*), $mei\text{-}W68^{1/DfBSC782}$, $mei\text{-}W68^{CD}$ and $mei\text{-}P22^{P22}$ 8-cell cysts stained for centromeres (CID, magenta), fusome (α-Spectrin, green), and DNA (DAPI, blue). (E) Graph plots the number of CID foci per nucleus in *WT*, $mei\text{-}W68^{1/Df27354}$, $mei\text{-}W68^{CD}$ and $mei\text{-}P22^{P22}$ 8-cell cysts. (*n*) is the number of cells analyzed for each genotype. ns $p \geq 0.05$ (two-tailed Student's t test comparing mutants with WT).

F-O, Centromeres II and III are paired in the mitotic region of *mei-W68* and *mei-P22* mutant cysts. (F-I) Confocal Z-section projections of *WT*, *mei-W68*$^{1/DfBSC782}$, *mei-W68*^{CD}and *mei-P22*^{P22} 8-cell cysts labeled with chromosome II centromeric probe (AACAC, green) and DNA (DAPI, blue). (J) Graph plots the percentage of paired chromosome II centromeres in *WT*, *mei-W68*$^{1/DfBSC782}$, *mei-W68*^{CD} and *mei-P22*^{P22} 8-cell cysts. (*n*) is the number of cells analyzed for each genotype. ns $p \geq 0.05$ (khi2 test comparing mutants with WT)

(K-N) Confocal Z-section projections of *WT*, *mei-W68*$^{1/DfBSC782}$, *mei-W68*^{CD} and *mei-P22*^{P22} 8-cell cysts labeled with chromosome III centromeric probe (dodeca, magenta) and DNA (DAPI, blue). Scale bar: 1 µm. (O) Graph plots the percentage of paired chromosome III centromeres in *WT*, *mei-W68*$^{1/DfBSC782}$, *mei-W68*^{CD2} and *mei-P22*^{P22} 8-cell cysts. (*n*) is the number of cells analyzed for each genotype. ns $p \geq 0.05$ (khi2 test comparing mutants with WT)

Scale bar: 5 µm in A-E; 1 µm in F-O.

Figure 5. *sunn, c(2)M, Nipped-B and SA* are dispensable for 8-cell cyst chromosome pairing in females.

(A-D) Confocal Z-section projections of *nos>sh-w*, *nos>sh-sunn, nos>sh-c(2)M, nos>sh-Nipped-B* and *nos>sh-SA* 8-cell cysts stained for centromeres (CID, magenta), fusome (α-Spectrin, green), and DNA (DAPI, blue). (E) Graph plots the number of CID foci per nucleus in *nos>sh-w*, *nos>sh-sunn, nos>sh-c(2)M, nos>sh-Nipped-B* and *nos>sh-SA* 8-cell cysts. (*n*) is the number of cells analyzed for each genotype. ns $p \geq 0.05$ (two-tailed Student's t test comparing *nos>sh-sunn, nos>sh-c(2)M, nos>sh-Nipped-B* and *nos>sh-SA* with *nos>sh-w*).

Scale bar: 5 µm.

Figure 6. Rpa-70 foci are not detected in the pre-meiotic region of *Drosophila*.

(A, A') Confocal Z-section projection of *RpA-70 EGFP* germarium (A, green; A', white) stained for the fusome (α-Spectrin, magenta). Note that RpA-70 EGFP is evenly distributed in the germline nucleoplasm with rare chromatin foci. Scale bar; 10 µm

(B, B') Confocal Z-section projections of *RpA-70 EGFP, spn-D*^{2} germarium (B, green; B', white) stained for the fusome (α-Spectrin, magenta). In a *spn-D*^{2} mutant germarium, many RpA-70 EGFP foci are detectable in region 2 and in older egg chambers, here shown region 3. Scale bar; 10 µm. The yellow dashed line delimits the boundary of mitotic and meiotic regions, with an 8-cell cyst and a 16-cell cyst, respectively, labelled with white dashed lines. (C) Mean

number of RpA-70 foci per cell counted in the mitotic 8cc (staged with α-Spectrin) and meiotic pro-oocytes (staged with C(3)G in early 2A, late 2B and 2B regions) of *RpA-70 EGFP* control, *RpA-70 EGFP, spn-D*^{2} and in *mei-W68*$^{1/DfBSC782}$*; RpA-70 EGFP, spn-D*^{2}. The number of analyzed cells for each genetic context is labelled as *n/n/n/n*.

(D-F') Confocal Z-section projections of *RpA-70 EGFP* (D, green; D', white), *RpA-70 EGFP; spn-D*^{2} (E, green; E', white) and *mei-W68*$^{1/DfBSC782}$*; RpA-70 EGFP, spn-D*^{2} (F, green; F', white) stained for ɣ-H2Av (magenta) and for synaptonemal complex (C(3)G, white). Note that the number of RpA-70 EGFP foci in region 2 is greatly reduced in *mei-W68*$^{1/k05603}$; *spn-D*^{2} mutant cells (compare E' and F'). Scale bar; 10 μm

(G-I') Confocal Z-section projections of selected pro-oocyte nuclei of cysts from *RpA-70 EGFP* (G, green; G', white), *RpA-70 EGFP; spn-D*^{2} (H, green; H', white) and *mei-W68*$^{1/DfBSC782}$*; RpA-70 EGFP, spn-D*^{2} (I, green; I', white) stained for synaptonemal complex (C(3)G, magenta) and DNA (DAPI, blue). Scale bar; 1 μm.

Figure S1. Progression of germ cells in Wcd-RFP germarium.

Confocal Z-section projections of germaria from wild type (A) and bam-GFP; nos>wcd-RFP (B) stained for ORB (white). Note that ORB localization in the meiotic region and in stage 2 is similar in both genotypes . Scale bar; 20 μm

Confocal Z-section projections of germaria from wild type (C) and bam-GFP; nos>wcd-RFP (D) stained for C(3)G (green) and DNA (DAPI, blue). Note that C(3)G is restricted to the selected oocyte (oocyte I) in meiotic region 3 and stage 2 in both genotypes (arrowheads, C and D) , but the synaptonemal complex is not completely resolved in the second pro-oocyte (pro-oocyte II) in nos>wcd-RFP (open arrowheads, D). Scale bar; 20 μm

(E) Graph plots C(3)G Fluorescence Intensity in the mitotic region and in the meiotic region 2 (WT, green, nos>wcd-RFP, magenta), meiotic region 3 and stage 2 (WT pro-oocyte I, green, WT pro-oocyte II , blue, nos>wcd-RFP pro-oocyte I, magenta and nos>wcd-RFP pro-oocyte II, grey). NS $p \geq 0.05$, * $p \leq 0.05$ (Mann-Whitney U-test). Number of samples analysed are below the bars.

(F) Graph plots the number of cysts in region 2 in wild type and bam-GFP, nos>wcd-RFP calculated using spectrin antibody labelling (not shown) . NS $p \geq 0.05$ (Mann-Whitney U-test). (*n*) is the number of germarium analyzed for each genotype.

Figure S2. *mei-W68* mRNA signal is detected above background levels in the meiotic and mitotic regions.

(A, A') Confocal Z-section projection of a *WT* germarium labelled for *mei-W68* mRNA by HCR *in situ* hybridization using *mei-W68* HCR-initiator probes (A, green; A', white). The yellow dashed line delimits the boundary of mitotic and meiotic regions. α-Spectrin antibody labelling is in magenta. Scale bar: 10 μm.

(B, B') Confocal Z-section projection of a *WT* germarium labelled by HCR *in situ* hybridization but excluding the HCR-initiator probes (compare with A, green; A', white). The yellow dashed line delimits the boundary of mitotic and meiotic regions. α-Spectrin antibody labelling is in magenta. Scale bar: 10 μm.

(C) Graph plots the Fluorescence Intensity in the mitotic region of WT germarium labelled by HCR *in situ* hybridization without (white) and with mei-W68 HCR-initiator probes (green). (*n*) is the number of germarium analyzed for each genotype.* $p \leq 0.05$ (Mann-Whitney U-test)

(D) Graph plots the Fluorescence Intensity in meiotic region of WT germarium labelled by HCR *in situ* hybridization without (white) and with mei-W68 HCR-initiator probes (green). (*n*) is the number of germarium analyzed for each genotype. **** $p \leq 0.0001$ (Mann-Whitney U-test).

Figure S3. *c(3)G*, *Nipped-B* and *mei-W68* mRNA expression in the meiotic region of Wcd-RFP germarium.

(A, B) Confocal Z-section projection of a *WT* (A) and *nos>wcd-RFP* (B) germarium labelled for *c(3)G* mRNA by HCR *in situ* hybridization (white). The yellow dashed line delimits the boundary of mitotic and meiotic regions. Scale bar: 10 μm. (C) Graph plots *mei-W68* mRNA Fluorescence Intensity in the meiotic region of WT (green) and *nos>wcd-RFP* (magenta) germarium labelled by HCR *in situ* hybridization. (*n*) is the number of germarium analyzed for each genotype. NS $p \geq 0.05$ (Mann-Whitney U-test).

(D, E) Confocal Z-section projection of a *WT* (D) and *nos>wcd-RFP* (E) germarium labelled for *Nipped-B* mRNA by HCR *in situ* hybridization (white). The yellow dashed line delimits the boundary of mitotic and meiotic regions. Scale bar: 10 μm. (F) Graph plots the *Nipped-B* mRNA Fluorescence Intensity in meiotic region of WT (green) and *nos>wcd-RFP* (magenta) germarium labelled by HCR *in situ* hybridization. (*n*) is the number of germarium analyzed for each genotype. NS $p \geq 0.05$ (Mann-Whitney U-test).

(G, H) Confocal Z-section projection of a *WT* (G) and *nos>wcd-RFP* (H) germarium labelled for *mei-W68* mRNA by HCR *in situ* hybridization (white). The yellow dashed line delimits the boundary of mitotic and meiotic regions. Scale bar: 10 µm. (I) Graph plots the *mei-W68* mRNA Fluorescence Intensity in the meiotic region of WT (green) and *nos>wcd-RFP* (magenta) germarium labelled by HCR *in situ* hybridization. (*n*) is the number of germarium analyzed for each genotype. NS $p \geq 0.05$ (Mann-Whitney U-test).

Figure S4 Mei-W68 reagents

(A) Schematic representation of *Drosophila melanogaster mei-W68* locus showing neighbouring genes CG7744 and *par-1* (top in grey). Enlargement of *mei-W68* and *par-1 RNA* showing introns (black acute lines for *mei-W68* and dashed lines for *par-1*), untranslated (magenta box) and translated regions (green box). Triangle represents $mei\text{-}W68^{1}$ insertion site of approximately 5kb (McKim and Hayashi-Hagihara). Positions of set of primers A, B and C used for RT-PCR are indicated .

(B) RT-PCR gene expression levels of $mei\text{-}W68^{1/DfBSC782}$ using primers A, B relative to *WT.*

(C) Representation of Mei-W68 catalytic (magenta box) and TOPRIM domains (blue box). $Mei\text{-}W68^{CD}$ is a substitution in the catalytic domain of the two conserved Tyrosine (Y80Y81) into Phenylalanine (*F80*F81). $Mei\text{-}W68^{HA}$ is tagged at the C-terminus with HA (green box) connected by a linker to His (yellow box)

Figure S5. Absence of DSBs in $Mei\text{-}W68^{HA}$ flies

Confocal Z-section projections of wild type (A, A'), $mei\text{-}W68^{HA}$/+ (B, B') and $mei\text{-}W68^{HA}$/ $mei\text{-}W68^{HA}$ (C, C') germaria stained for DSBs (ɣ-H2Av, magenta), fusome (α-Spectrin, green) and DNA (DAPI, blue). The yellow dashed line delimits the boundary of mitotic and meiotic regions. Note that DSBs are absent in $mei\text{-}W68^{HA}$/ $mei\text{-}W68^{HA}$. Scale bar; 10 µm

Figure S6. Mei-W68 and Mei-P22 mutant flies do not produce DSBs

Confocal Z-section projections of wild type (A, A'), $mei\text{-}W68^{1/DfBSC782}$ (B, B'), $mei\text{-}W68^{CD/CD}$ (C, C') and $mei\text{-}P22^{P22/P22}$ (D, D') germaria stained for DSBs (ɣ-H2Av, magenta), fusome (α-Spectrin, green) and DNA (DAPI, blue). The yellow dashed line delimits the boundary of mitotic and meiotic regions. Note that DSBs are absent in all the mutants. Scale bar; 10 µm

Figure S7. RPA::GFP foci transiently overlap with ɣ-H2Av.

(A-A'') Confocal Z-section projection of *RpA-70 EGFP* pro-oocyte stained for DSBs (ɣ-H2Av, A, A'', magenta) and DNA (DAPI, A'',blue). GFP is in green (A', A''). Scale bar= 10 µm.
(B) Line profile plots the normalized intensity for ɣ-H2Av (magenta) and RPA::GFP (green) from A'' (yellow dashed line). The RPA::GFP peak partially overlaps with the ɣ-H2Av peak on the right side, but not with the ɣ-H2Av on the left side.
(C-C'') Confocal Z-section projection of *RpA-70 EGFP; spn-D*^{2} pro-oocyte stained for DSBs (ɣ-H2Av, C, C'', magenta) and DNA (DAPI, C'',blue). GFP is in green (C'', C''). Scale bar= 10 µm.
(D) Line profile plots the normalized intensity for ɣ-H2Av (magenta) and RPA::GFP (green) from C'' (yellow dashed line). The two RPA::GFP peaks overlap with the two ɣ-H2Av peaks.
(E) Percentages of ɣ-H2Av overlapping with RPA::GFP (magenta) and RPA::GFP overlapping with ɣ-H2Av (green) in *RpA-70 EGFP* and *RpA-70 EGFP; spn-D*^{2} pro-oocytes. The number of analyzed nuclei is indicated under each genotype.

Movie S1: Live-imaging of RPA::GFP in wild type germarium. Maximum intensity projection. (1 frame each 3 mn).

Movie S2: Live-imaging of RPA::GFP in *spn-D*^{2} mutant germarium. Maximum intensity projection. (1 frame each 3 mn).

FIGURE

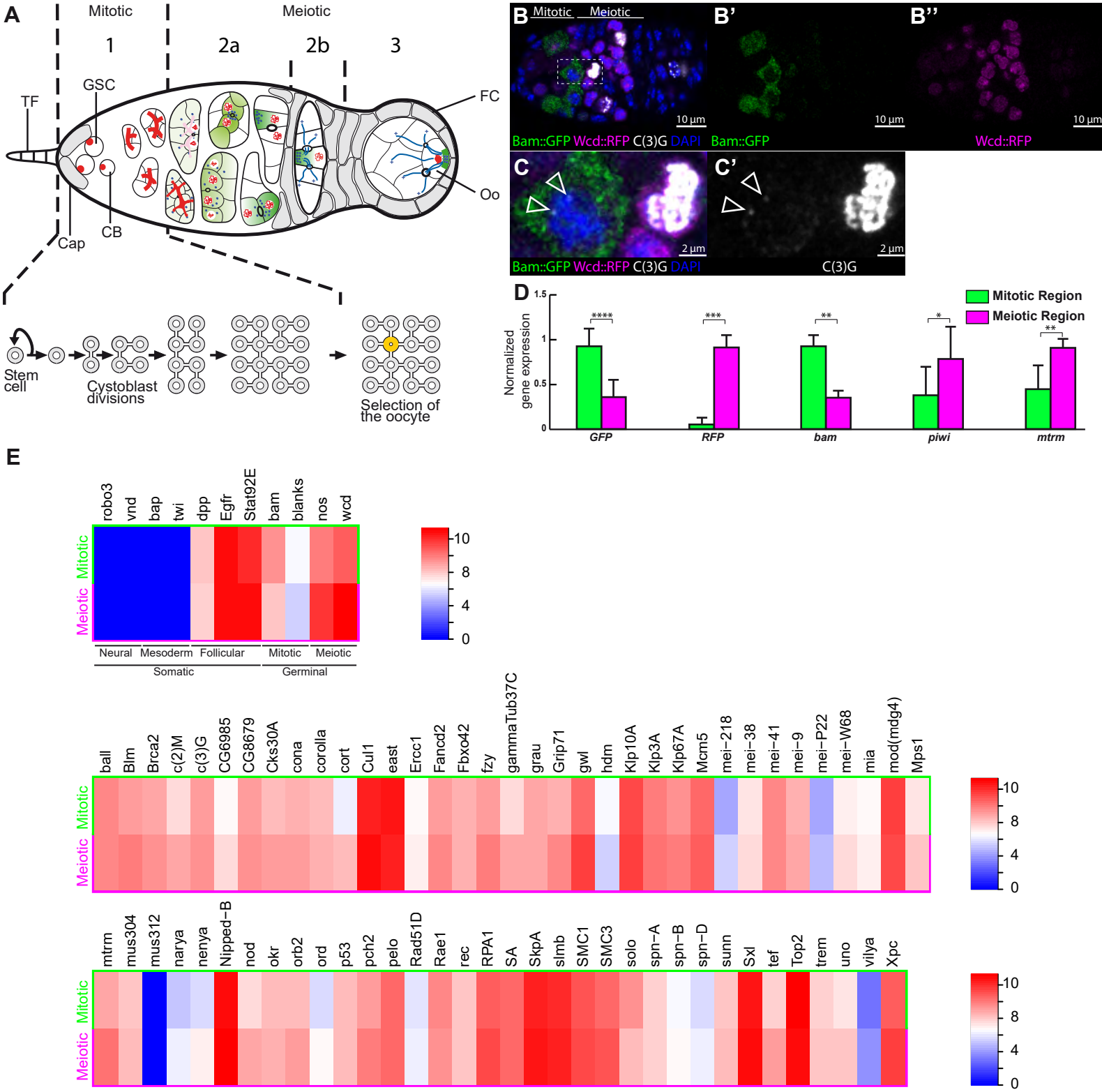

FIGURE 2

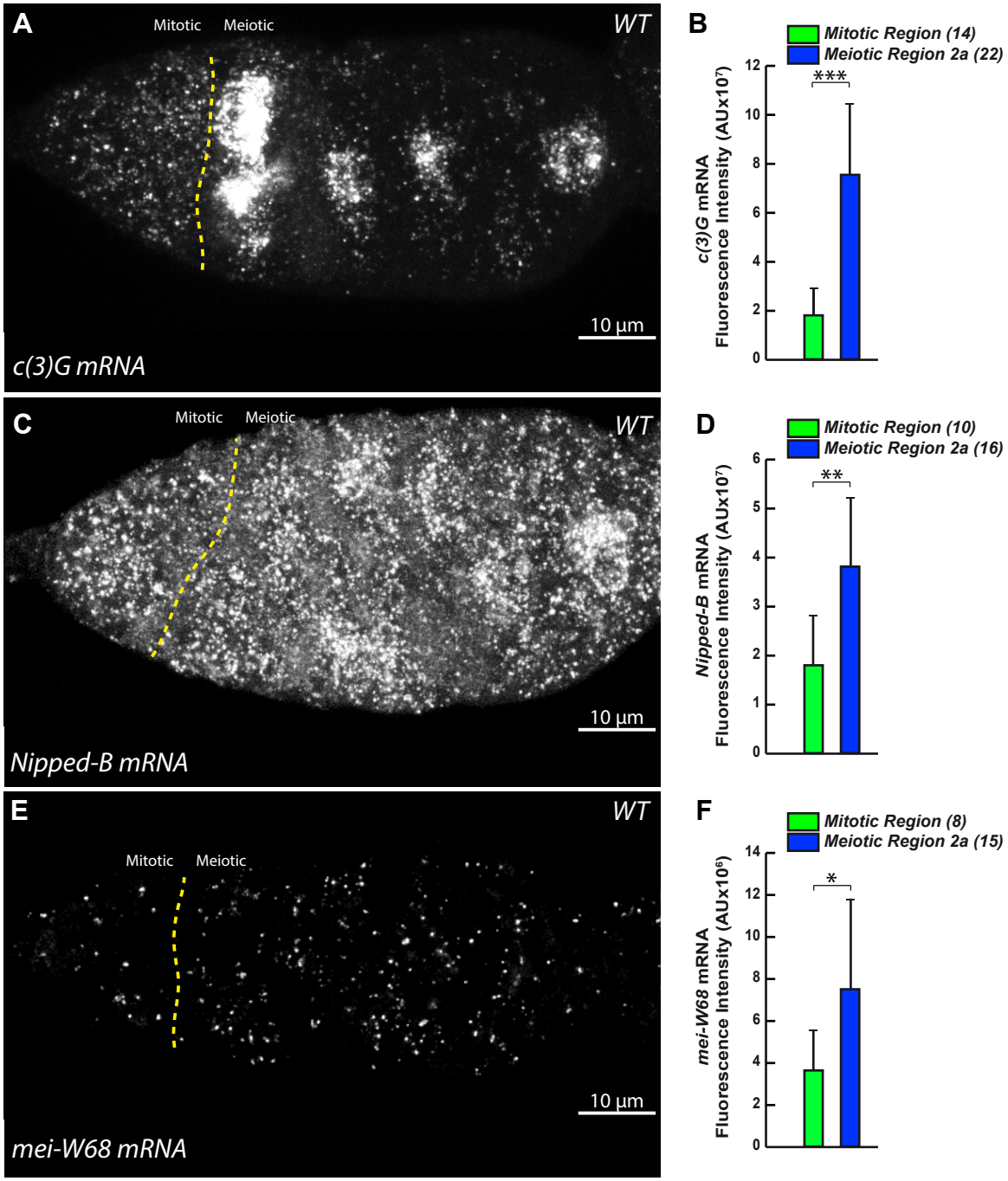

FIGURE 3

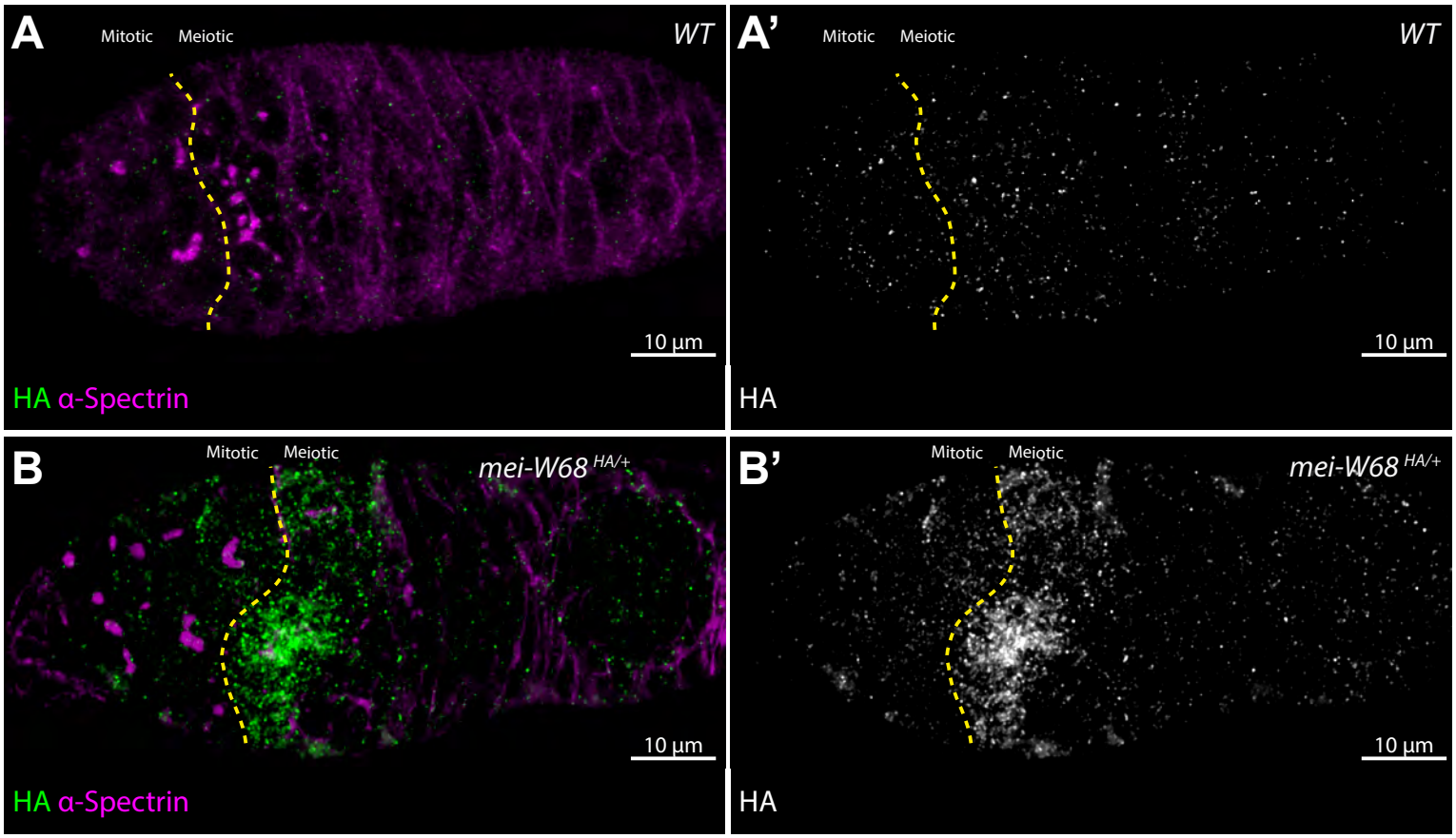

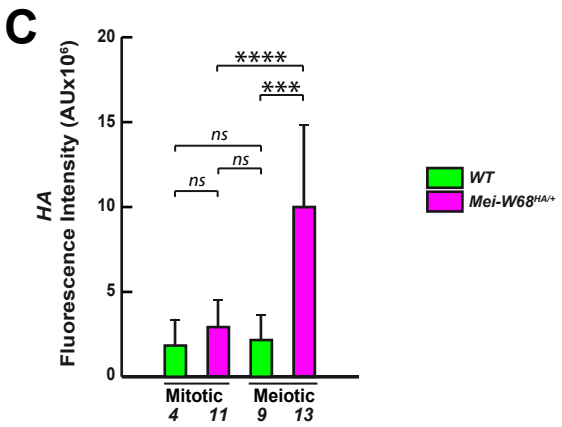

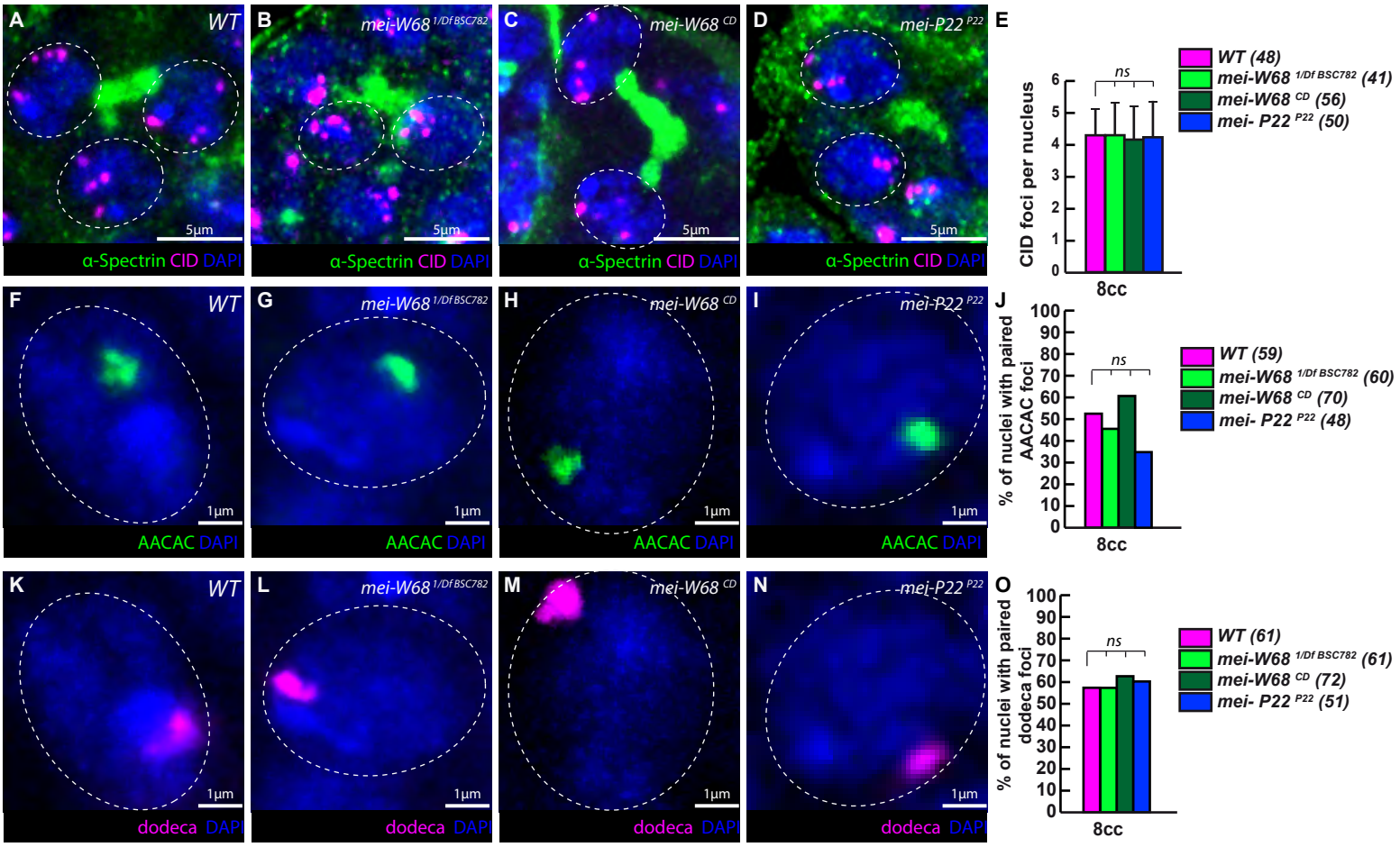

Figure 5

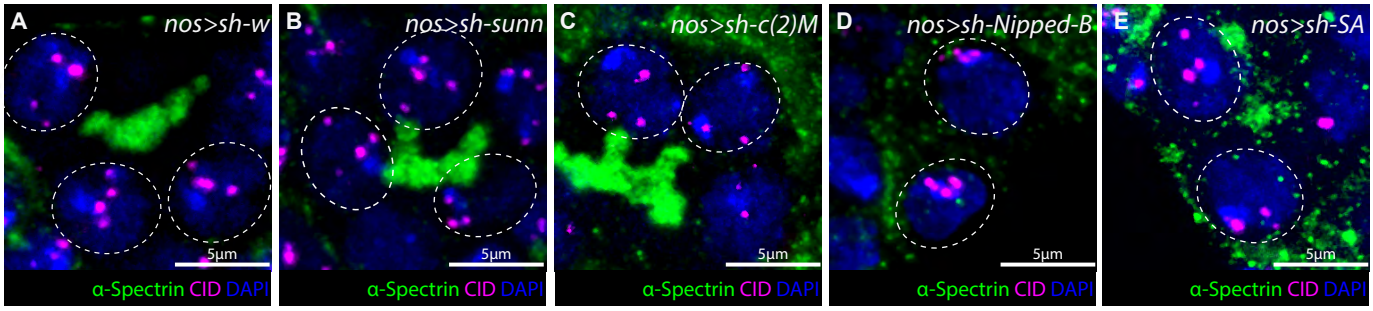

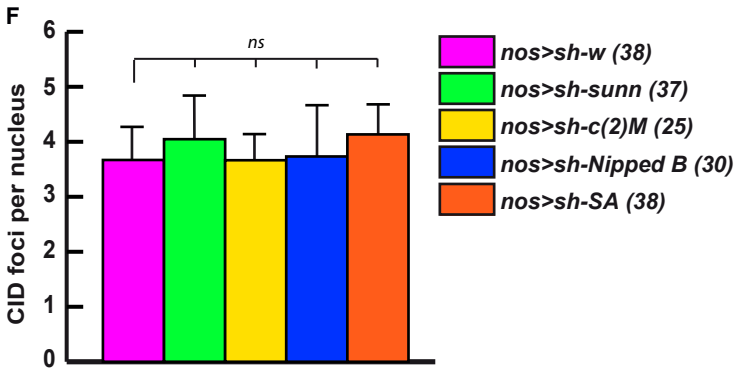

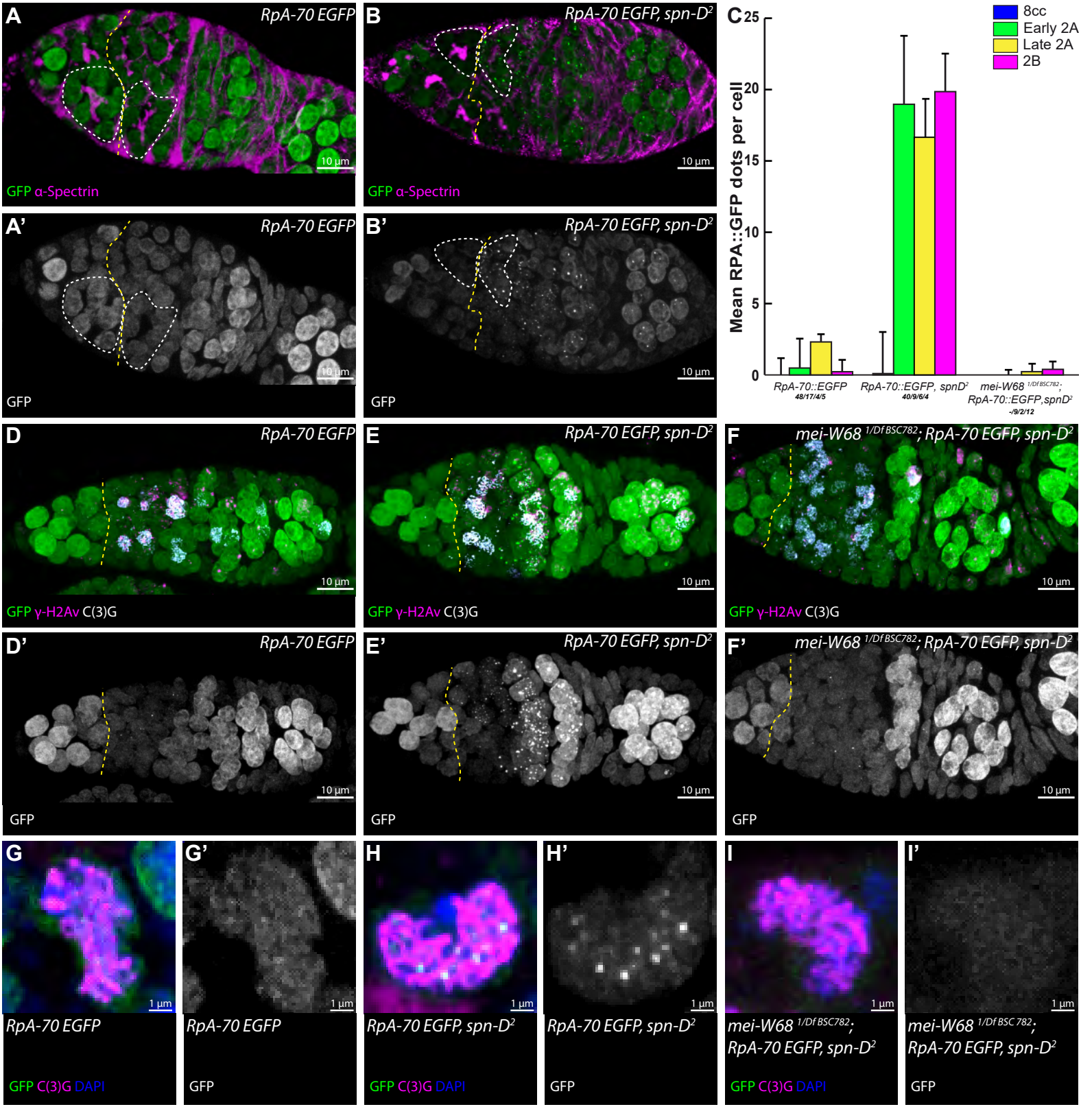

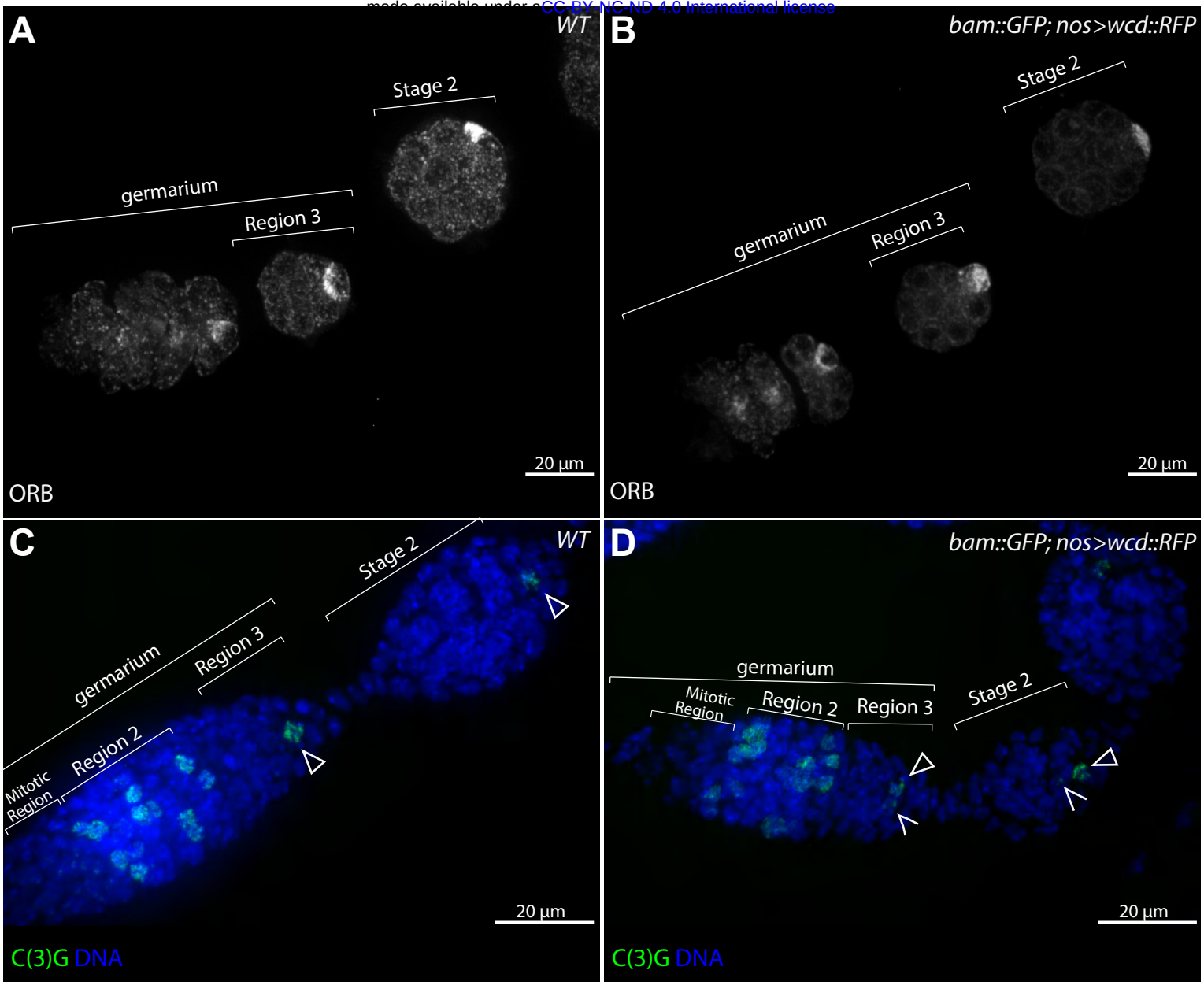

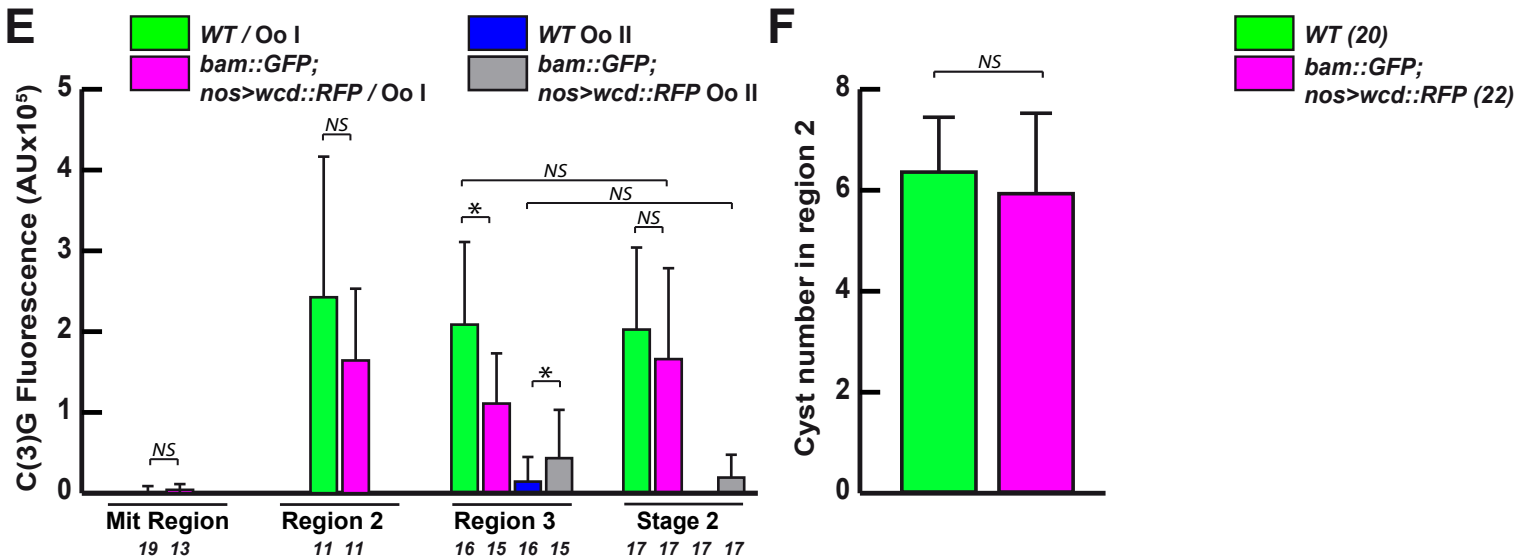

FIGURE S2

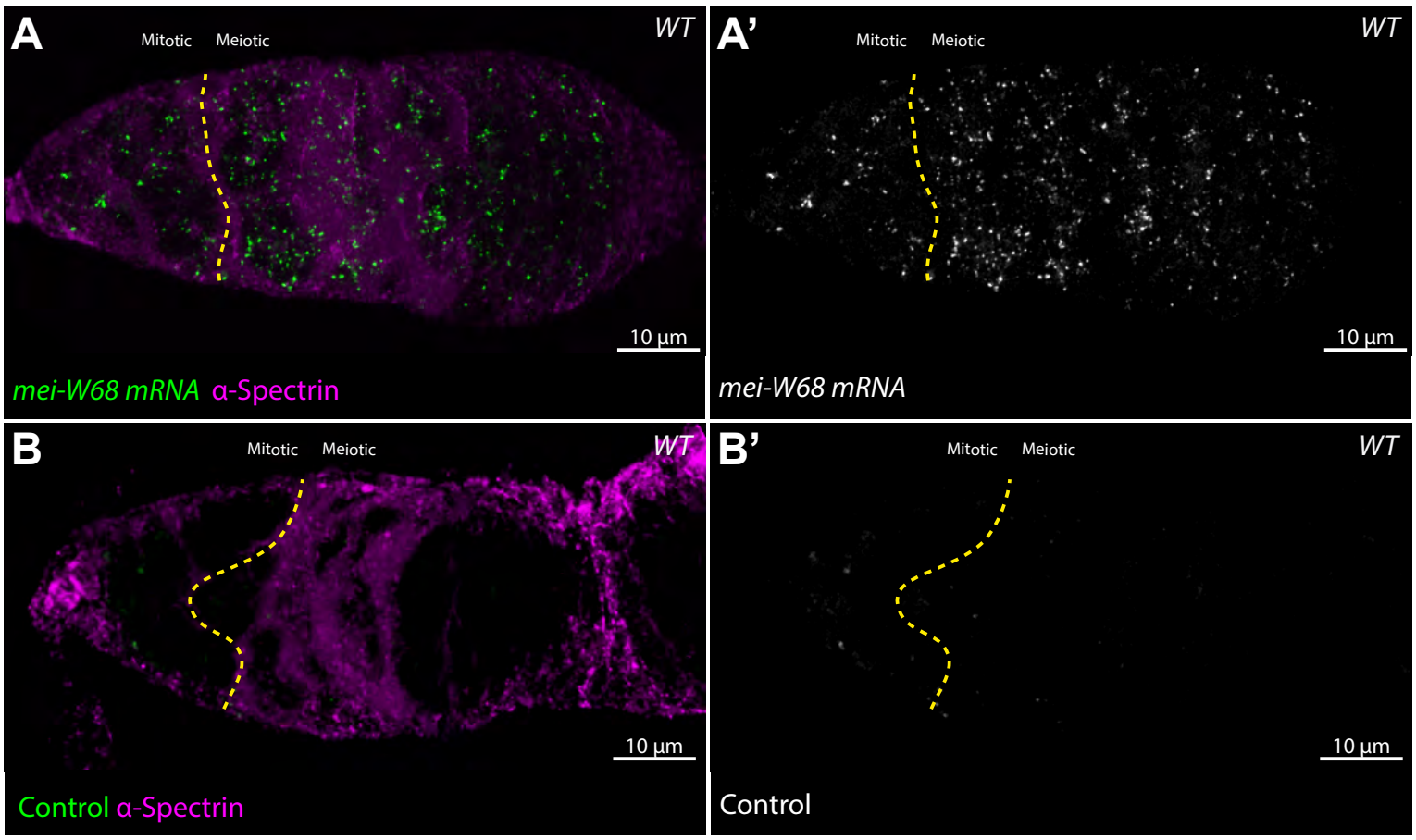

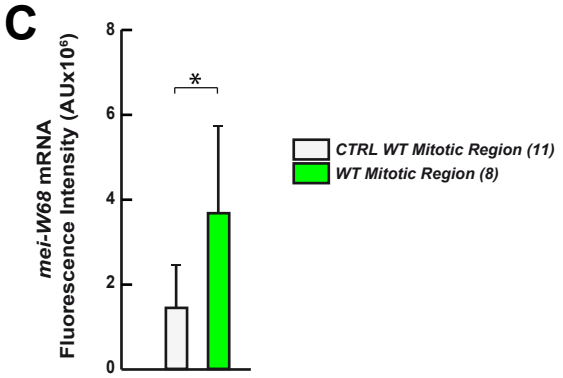

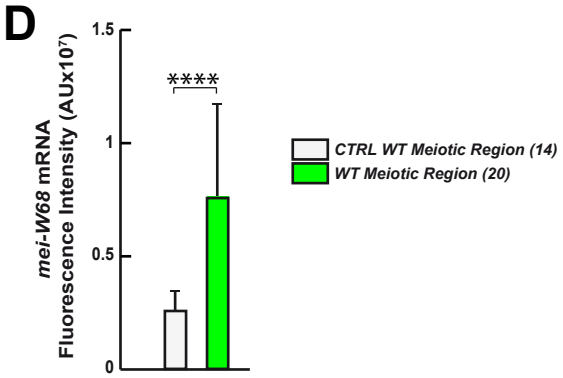

FIGURE S3

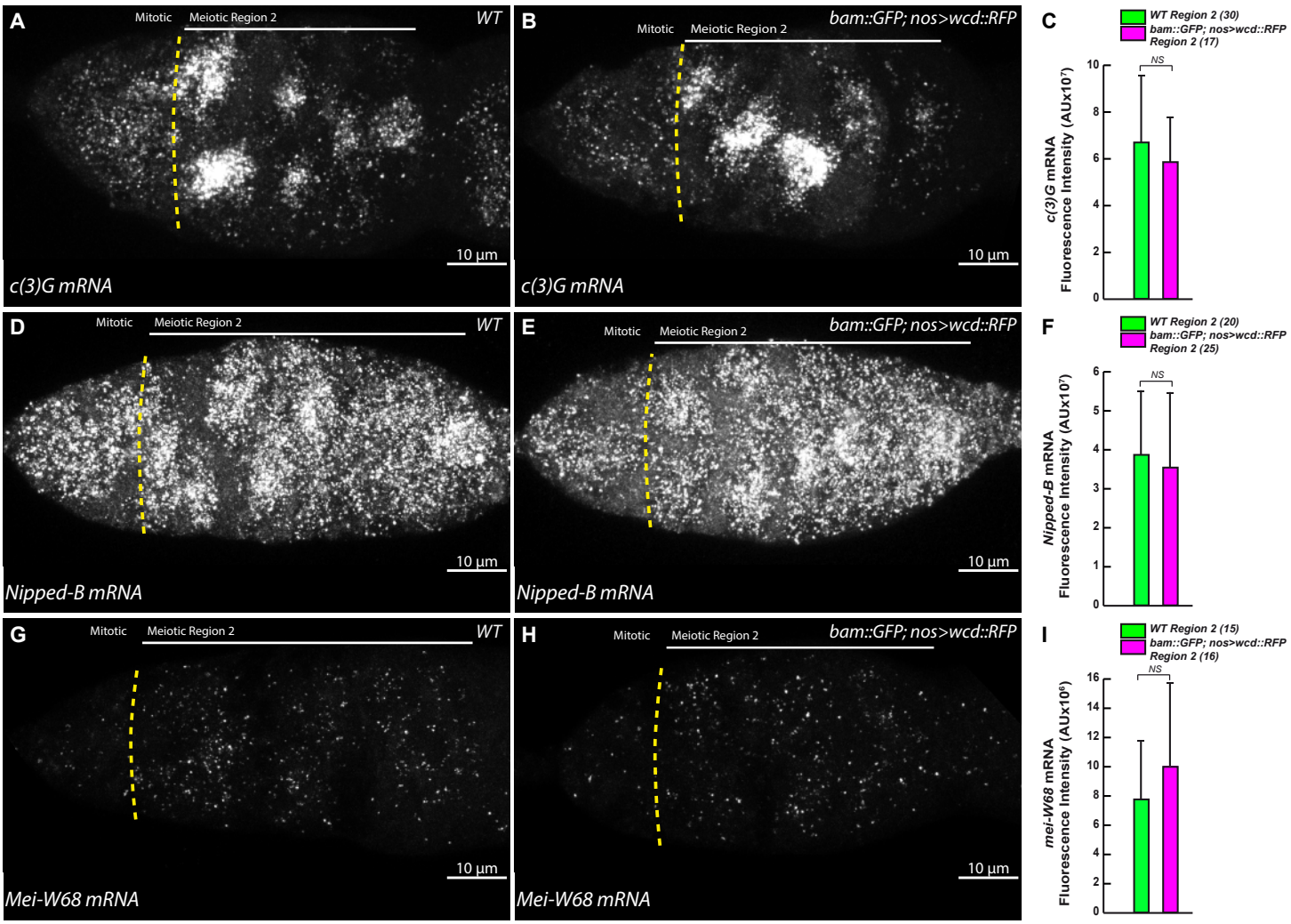

Figure S4

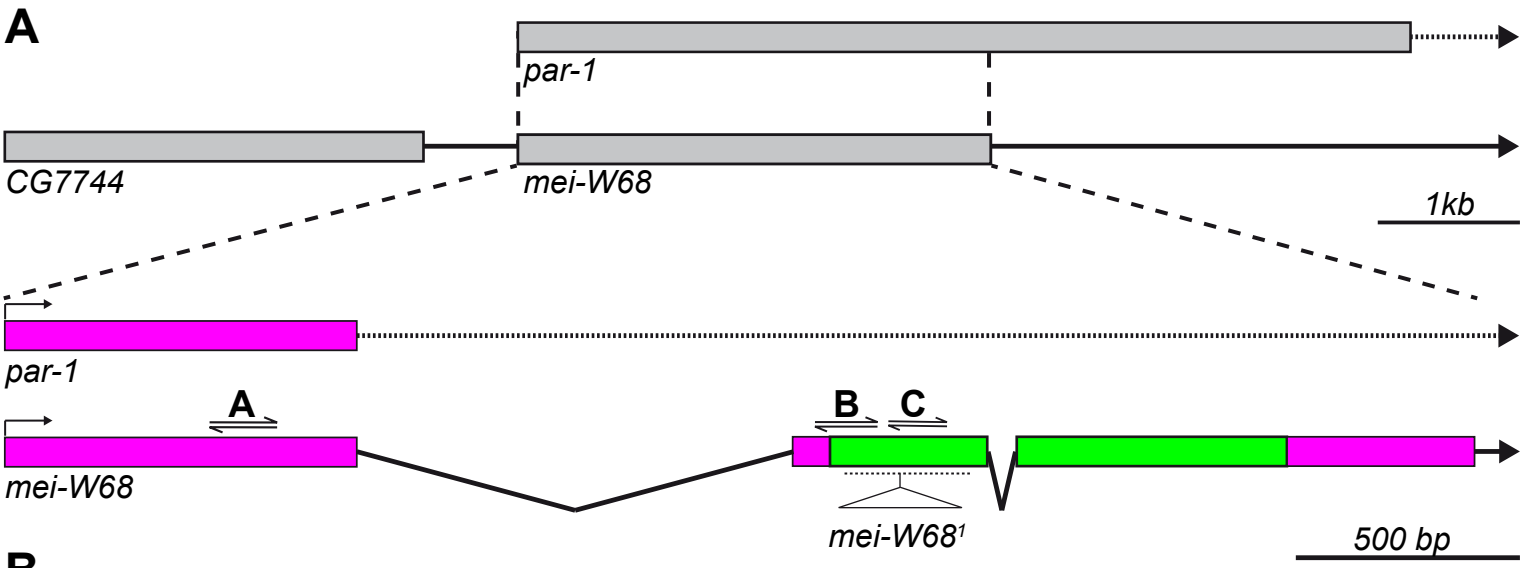

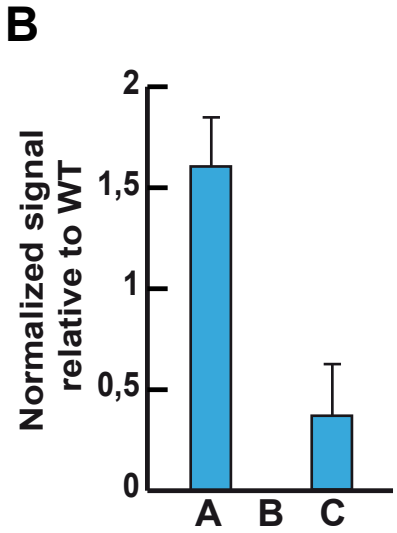

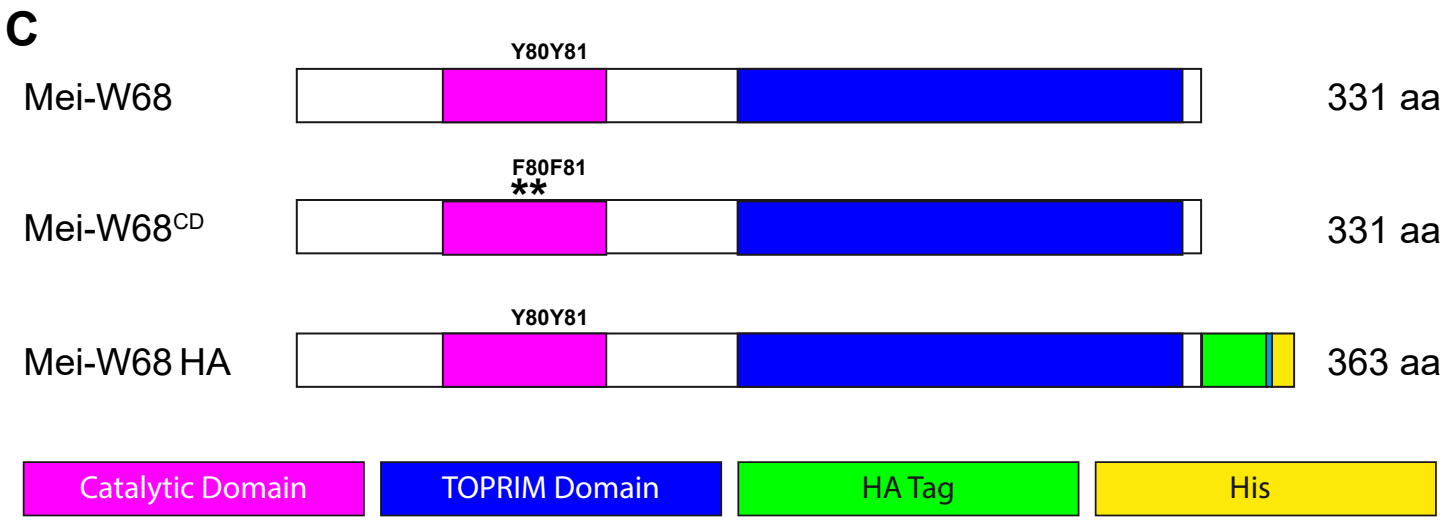

FIGURE S5

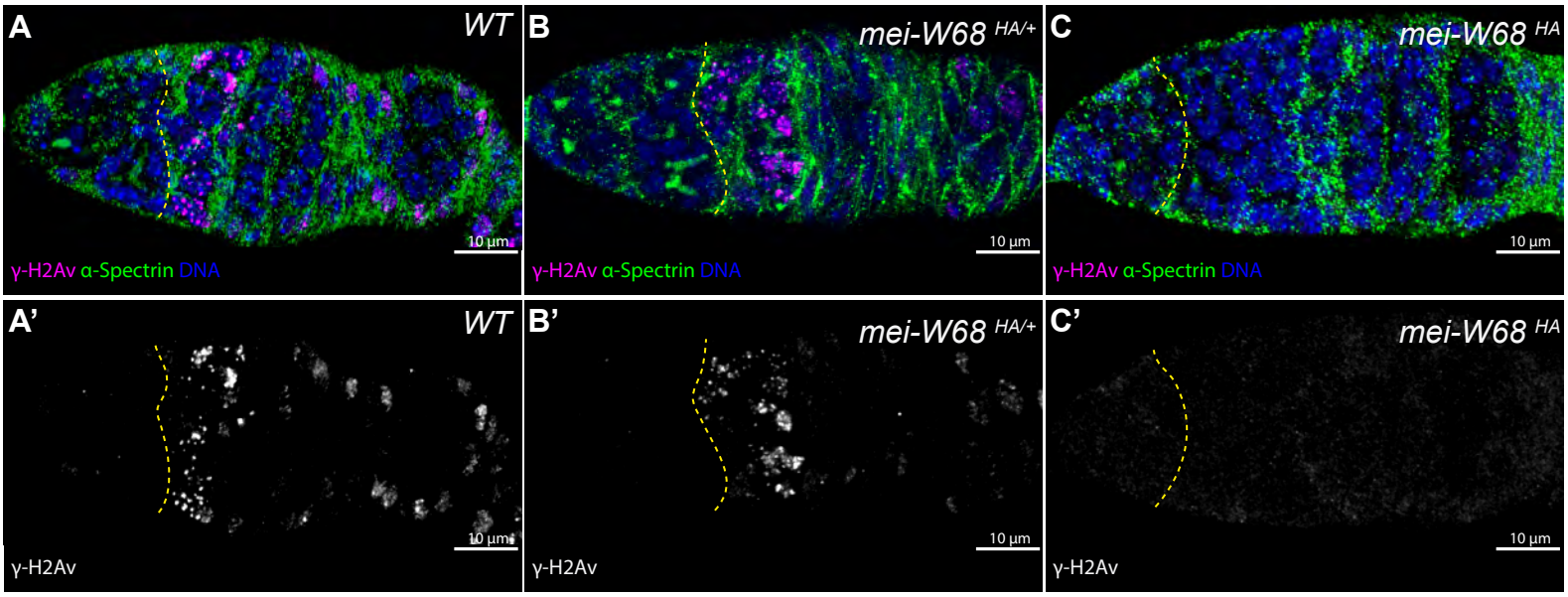

Figure S6

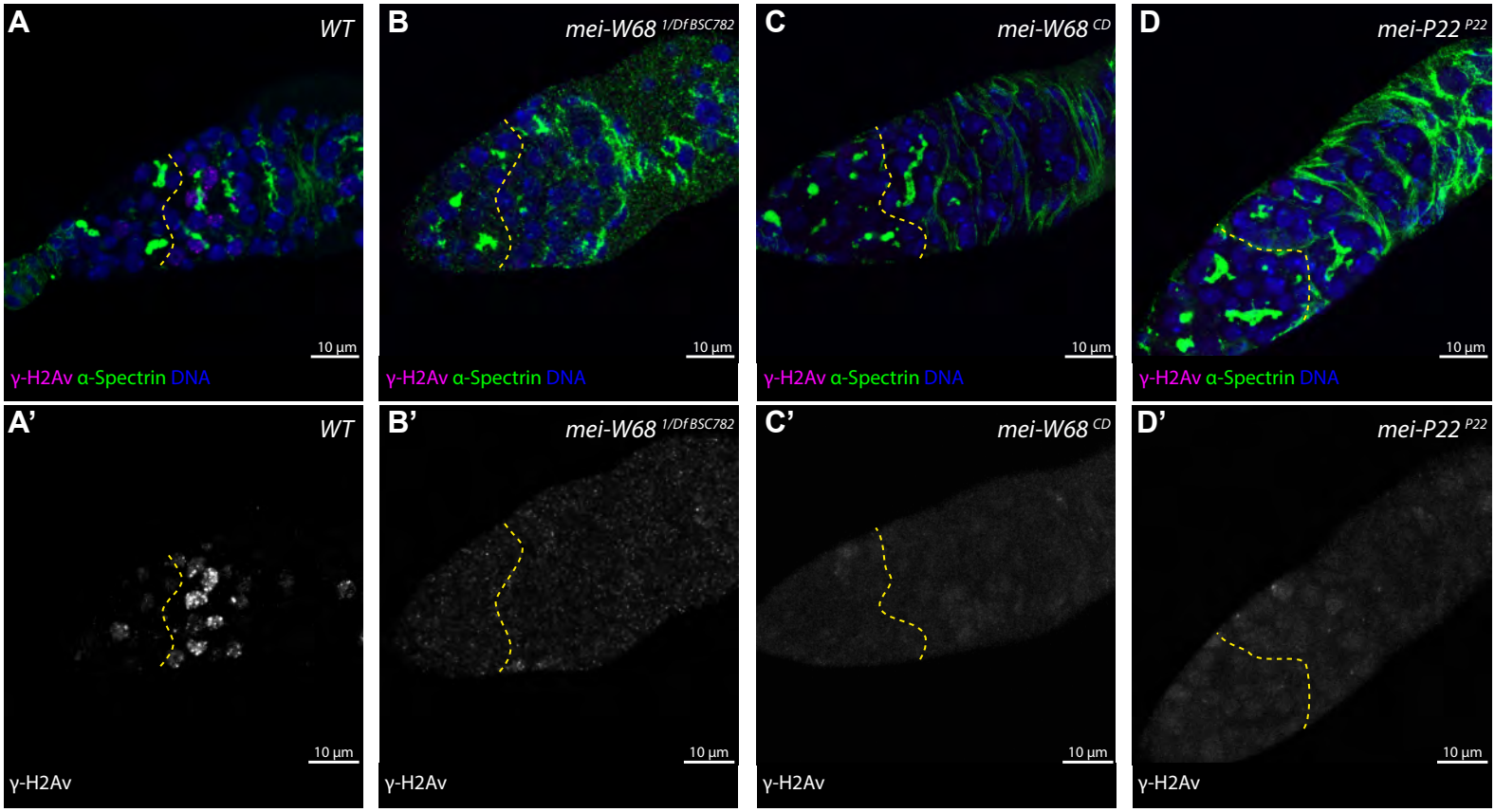

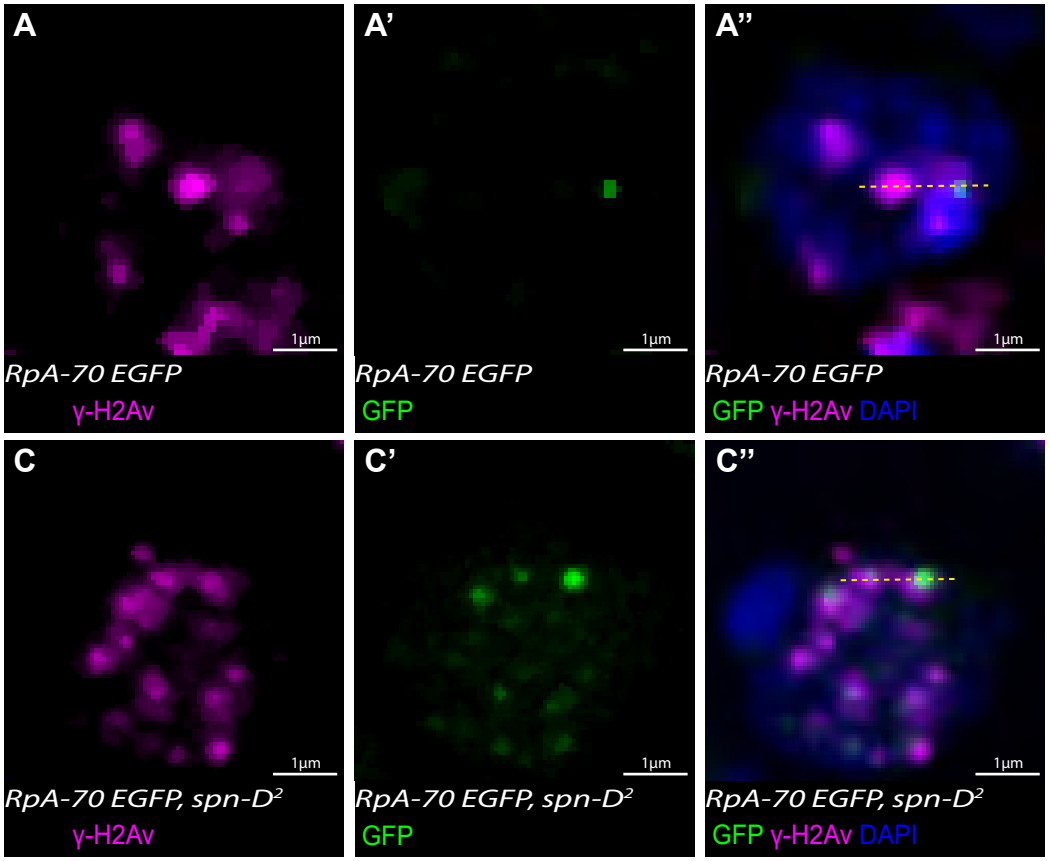

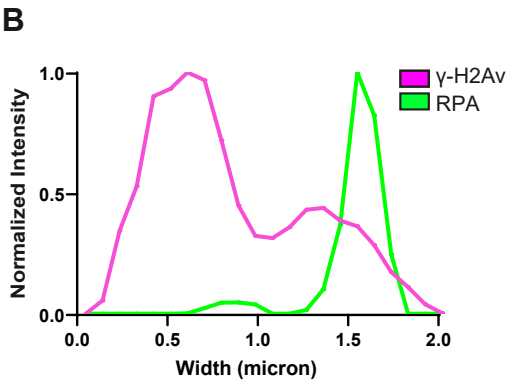

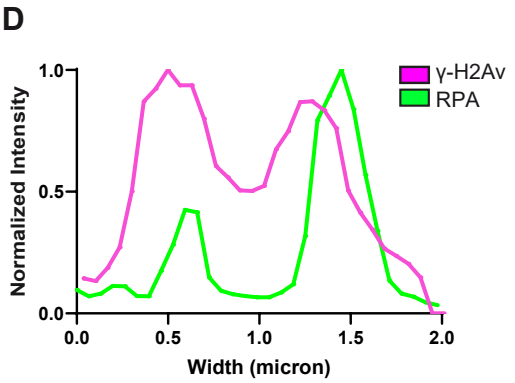

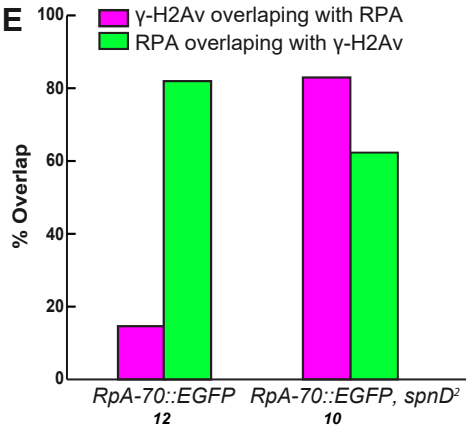

Supplemental Table S1 - Meiotic genes are expressed in mitotic region

Tab 1 - Meiotic genes compiled from FlyBase GO term (GO: 0007127), excluding genes identified as male-specific. Included in the list were sorting (bam, blanks, nos and wcd), and tissue contamination (robo3, vnd, bap, twi, dpp, Egfr and Stat92E) controls

Table columns: GeneID; BaseMean_MIT; BaseMean_MEI; Fold-Change (Green <1, Red > 1); Pvalue (

GeneID	basemeanMITOSIS	basemeanMEIOSIS	FC	Pvalue	Gene8name
robo3	0	0	#DIV/0!	NA	*robo3*
vnd	0	0	#DIV/0!	NA	*vnd*
bap	0	0	#DIV/0!	NA	*bap*
twi	0	0	#DIV/0!	NA	*twi*
dpp	281,8288704	213,3202867	0,756914245	2,17E-01	*dpp*
Egfr	7807,632041	7543,856239	0,966215646	8,58E-01	*Egfr*
Stat92E	4711,71483	7212,509959	1,530761139	5,32E-03	*Stat92E*
bam	730,6639492	269,4691812	0,368800434	5,46E-02	*bam*
blanks	91,09768961	41,21081093	0,452380418	1,89E-01	*blanks*
nos	990,9177712	3738,674353	3,772941067	3,20E-20	*nos*
wcd	1769,707111	9471,017057	5,35174267	5,61E-08	*wcd*
ball	880,2963858	803,6406877	0,912920581	7,36E-01	*ball*
Blm	607,2924757	1034,604345	1,703634387	9,18E-03	*Blm*
Brca2	479,6619339	758,0115539	1,580303752	8,08E-03	*Brca2*
c(2)M	194,7446541	442,24078	2,27087507	5,31E-03	*c(2)M*
c(3)G	628,2986357	750,4303538	1,194384822	5,84E-01	*c(3)G*
CG6985	100,9792309	193,2552985	1,913812344	1,37E-02	*CG6985*
CG8679	589,0147164	678,94307	1,152675903	4,09E-01	*CG8679*
Cks30A	336,3332698	583,3106724	1,734323437	4,31E-02	*Cks30A*
cona	422,7600976	576,8662139	1,364523798	5,68E-01	*cona*
corolla	344,2825957	372,9445962	1,083251378	8,51E-01	*corolla*
cort	78,4953099	317,7518291	4,048035857	3,08E-07	*cort*
Cul1	5606,077582	7551,760477	1,347066709	7,10E-02	*Cul1*
east	6184,65249	5692,575824	0,920435842	6,83E-01	*east*
Ercc1	104,2694458	142,7652119	1,369195077	2,66E-01	*Ercc1*
Fancd2	568,2569004	824,1802943	1,45036566	1,96E-01	*Fancd2*
Fbxo42	363,6324801	372,1317804	1,023373326	9,37E-01	*Fbxo42*
fzy	574,9221203	978,6279939	1,702192279	3,16E-02	*fzy*
gammaTub37C	208,4513745	478,9412384	2,29761612	8,08E-04	*gammaTub37C*
grau	485,1535591	485,7075555	1,001141899	9,97E-01	*grau*
Grip71	432,1083855	818,9286825	1,895192757	5,97E-03	*Grip71*
gwl	1337,511593	2862,755907	2,140359697	8,36E-03	*gwl*
hdm	91,7340959	39,66825137	0,432426471	2,35E-01	*hdm*
Klp10A	2626,397374	2956,55932	1,12570906	4,57E-01	*Klp10A*
Klp3A	953,7489433	1200,350565	1,258560309	3,09E-01	*Klp3A*
Klp67A	686,0465332	1004,233086	1,463797333	1,69E-01	*Klp67A*
Mcm5	1541,39132	1639,713515	1,063787952	7,79E-01	*Mcm5*
mei-218	21,00815102	38,96380404	1,85469935	1,78E-01	*mei-218*
mei-38	152,8540135	176,3177538	1,153504247	7,92E-01	*mei-38*
mei-41	793,5206952	844,259554	1,063941444	8,12E-01	*mei-41*
mei-9	412,6763782	470,077229	1,139094103	5,01E-01	*mei-9*
mei-P22	18,73142554	29,97026408	1,599999104	6,23E-01	*mei-P22*
mei-W68	120,0394972	176,3007259	1,468689306	2,65E-01	*mei-W68*
mia	106,2384582	134,703881	1,267938967	5,78E-01	*mia*
mod(mdg4)	2900,984966	2430,648854	0,8378702	3,45E-01	*mod(mdg4)*
Mps1	153,232169	278,7081998	1,818862198	5,64E-02	*Mps1*
mtrm	437,1554699	1119,012534	2,559758738	6,22E-08	*mtrm*
mus304	271,1724424	359,7809682	1,326760806	2,12E-01	*mus304*
mus312	0	0	#DIV/0!	NA	*mus312*

narya	35,97019178	70,21136504	1,951931907	2,02E-01	*narya*
nenya	48,80659677	121,0444724	2,480084258	1,00E-02	*nenya*
Nipped-B	7428,242749	10050,8051	1,35305286	8,79E-02	*Nipped-B*
nod	181,6257799	522,1903895	2,875089592	3,02E-04	*nod*
okr	330,8717399	399,6599534	1,207899936	5,13E-01	*okr*
orb2	334,2960075	531,9504851	1,591255872	9,97E-02	*orb2*
ord	48,908937	100,6944375	2,058814681	7,67E-02	*ord*
p53	345,1952124	346,8628188	1,004830908	9,80E-01	*p53*
pch2	617,9542897	936,8238603	1,516008346	8,10E-02	*pch2*
pelo	1379,40458	1462,625958	1,060331377	7,43E-01	*pelo*
Rad51D	63,03231676	78,47929553	1,24506443	6,24E-01	*Rad51D*
Rae1	816,8423394	688,2189004	0,842535784	3,45E-01	*Rae1*
rec	294,5195615	277,5298231	0,942313718	8,92E-01	*rec*
RPA1	1803,562756	2357,140947	1,306935918	2,14E-01	*RPA1*
SA	1377,776629	1363,006843	0,989279985	9,56E-01	*SA*
SkpA	5509,782723	6513,064293	1,18209095	2,41E-01	*SkpA*
slmb	4602,087073	4858,358166	1,055685842	7,61E-01	*slmb*
SMC1	2195,496974	2392,540879	1,089749113	6,82E-01	*SMC1*
SMC3	1430,047804	1948,816202	1,362762977	1,54E-01	*SMC3*
solo	687,4800873	330,2416201	0,480365361	1,97E-01	*solo*
spn-A	216,8014786	239,8603438	1,106359354	6,49E-01	*spn-A*
spn-B	97,63089149	117,9593533	1,208217517	6,14E-01	*spn-B*
spn-D	48,55932791	82,19454918	1,692662413	2,16E-01	*spn-D*
sunn	271,0365832	303,0175888	1,117995162	8,05E-01	*sunn*
Sxl	6546,815137	7219,741937	1,102786895	5,01E-01	*Sxl*
tef	246,1993578	632,0700059	2,567309726	1,16E-04	*tef*
Top2	9818,887772	7933,941627	0,808028548	3,44E-01	*Top2*
trem	247,4028146	300,5448873	1,21479979	4,47E-01	*trem*
uno	156,3918711	297,0587735	1,899451496	6,58E-03	*uno*
vilya	6,761964214	12,47965379	1,845566376	5,71E-01	*vilya*
Xpc	1626,867463	3196,493288	1,964814812	6,06E-04	*Xpc*

t-test, Red < 0,1); Gene_name

Supplementary Table S5. *X*-NDJ in *nos>wcd-RFP* females

A. Sex chromosome NDJ :

Progeny:	Regular		Exceptional			
Maternal genotype	XX	XY	XXY	X0	Nc	% NDJ
WT	252	186	1	0	440	0.5
nos>wcdRFP/+	212	204	0	1	418	0.5
nos>UAS-GFP	234	237	0	0	471	0

Indicated females were crossed to *w/BsYy+* males. Surviving exceptional aneuploids are Bar-eyed *y/y/B^{s}Y* females and wild-type *yw/0* males

Percentage of *X*-NDJ: 100 x 2(X-NDJ progeny)/total progeny, where total progeny (Nc) was calculated as 2(X-NDJ progeny) + regular progeny (Gyuricza et al 2016).

Supplementary Table S6. NDJ in *mei-W68* mutant females

A. Sex chromosome NDJ Frequencies :

Progeny:	Regular		Exceptional			
Maternal genotype	XX	XY	XXY	XO	Nc	%NDJ
+/+	254	288	0	0	542	0
mei-W68^{1}/ Df^{27354}	166	118	78	44	528	46.21
mei-W68^{CD}	236	220	44	38	620	26.45
mei-W68^{HA}	193	166	25	53	515	30.29
mei-W68^{HA}/ Df^{27354}	218	207	68	68	697	39.02
mei-W68^{HA}/ +	325	323	0	3	654	0.92
mei-P22	197	209	44	41	576	29.51

Females with indicated second or third chromosome were crossed to *w/BsYy+* males. Surviving exceptional aneuploids are Bar-eyed *y/y/B^{s}Y* females and wild-type *yw/0* males. Percentage of X-NDJ: 100 x 2(X-NDJ progeny)/total progeny, where total progeny (Nc) was calculated as 2(X-NDJ progeny) + regular progeny (Gyuricza et al 2016)

B. 2nd chromosome NDJ Frequencies :

Maternal genotype :	Diplo-2	Nullo-2	F1/n
+/+	0	0	0
mei-W68^{1}/ Df^{27354}	103	42	3.62
mei-W68^{CD}	22	52	14.8
mei-W68^{HA}	84	73	7.85
mei-W68^{HA}/ Df^{27354}	55	35	4.5
mei-W68^{HA}/ +	0	0	0
mei-P22	3	4	1.4

Females with indicated second or third chromosome were crossed to *C(2)EN b^{1} pr^{1}* males.

F1/n is the frequency of NDJ/total number of females crossed.

Supplementary Table S7. *X*-NDJ in females mutant for meiotic genes

A. Sex chromosome NDJ :

Progeny:	Regular		Exceptional			
Maternal genotype	XX	XY	XXY	X0	Nc	% NDJ
nos>sh-w	393	169	0	1	564	0.35
nos>sh-sunn	322	313	29	24	741	14.30
nos>sh-c(2)M	172	157	15	15	389	15.42
nos>sh-Nipped-B	126	92	5	4	236	7.63
nos>sh-SA-1 [a]						

Indicated females were crossed to *w/BsYy+* males. Surviving exceptional aneuploids are Bar-eyed *y/y/B^{s}Y* females and wild-type *yw/0* males

Percentage of *X*-NDJ: 100 x 2(X-NDJ progeny)/total progeny, where total progeny (Nc) was calculated as 2(X-NDJ progeny) + regular progeny (Gyuricza et al. 2016)

[a] many embryonic lethal